Combinatorial drug-microenvironment interaction mapping reveals cell-extrinsic drug resistance mechanisms and clinically relevant patient subgroups in CLL

Short Title for Running Head:

Drug-microenvironment-genetic interactions in CLL

Peter-Martin Bruch*[1,2], Holly A. R. Giles*[1-4], Carolin Kolb[1,2], Sophie A. Herbst[1-3,5], Tina Becirovic[1], Tobias Roider[1-3], Junyan Lu[3], Sebastian Scheinost[5,7], Lena Wagner[5,7], Jennifer Huellein[3], Ivan Berest[3], Mark Kriegsmann[6], Katharina Kriegsmann[1], Christiane Zgorzelski[6], Peter Dreger[1], Judith B. Zaugg[2,3], Carsten Müller-Tidow[1,2], Thorsten Zenz[8], Wolfgang Huber*[2,3], Sascha Dietrich*[1-3,5]

1. Department of Medicine V, University of Heidelberg, Heidelberg, Germany
2. Molecular Medicine Partnership Unit (MMPU), Heidelberg, Germany
3. EMBL Heidelberg, Heidelberg, Germany
4. Collaboration for joint PhD degree between EMBL and Heidelberg University, Faculty of Biosciences, Heidelberg, Germany
5. German Cancer Research Center (DKFZ), Heidelberg, Germany
6. Institute of Pathology, University of Heidelberg, Heidelberg, Germany
7. National Center for Tumour Diseases, Heidelberg, Germany
8. Department of Hematology, University of Zürich, Zürich, Switzerland

Corresponding Author Details

Name: Sascha Dietrich

Address: Im Neuenheimer Feld 410, 69120 Heidelberg, Germany

Email: Sascha.Dietrich@med.uni-heidelberg.de

Phone: 06221/56-39894 06621/56-310977

Fax number: 06221/56-5736

Name: Wolfgang Huber

Address: Meyerhofstraße 1, 69117 Heidelberg, Germany

Email: wolfgang.huber@embl.de

Phone: +49 6221 387-8823

Fax number: +49 6221 387-8166

Abstract

The tumour microenvironment and genetic alterations collectively influence drug efficacy in cancer, but current evidence is limited to small scale studies and systematic analyses are lacking. We chose Chronic Lymphocytic Leukaemia (CLL), the most common leukaemia in adults, as a model disease to study this complex interplay systematically.

We performed a combinatorial assay using 12 drugs individually co-applied with each of 17 microenvironmental stimuli in 192 primary CLL samples, generating a comprehensive map of drug-microenvironment interactions in CLL. This data was combined with whole-exome sequencing, DNA-methylation, RNA-sequencing and copy number variant annotation.

Our assay identified four distinct CLL subgroups that differed in their responses to the panel of microenvironmental stimuli. These subgroups were characterized by distinct clinical outcomes independently of known prognostic markers. We investigated the effect of CLL-specific recurrent genetic alterations on microenvironmental responses and identified trisomy 12 as an amplifier of multiple microenvironmental stimuli. We further quantified the impact of microenvironmental stimuli on drug response, confirmed known interactions such as Interleukin (IL) 4 mediated resistance to B cell receptor (BCR) inhibitors, and identified new interactions such as Interferon-γ induced resistance to BCR inhibitors. Finally, we identified interactions which were limited to genetic subgroups. Resistance to chemotherapeutics, such as Fludarabine, induced by Toll-Like Receptor (TLR) agonists could be observed in IGHV unmutated patient samples and IGHV mutated samples with trisomy 12. In-vivo relevance was investigated in CLL-infiltrated lymph nodes, which showed increased IL4 and TLR signalling activity compared to healthy samples ($p<0.001$). High IL4 activity in lymph nodes correlated with faster disease progression ($p=0.038$).

We provide a publicly available resource (www.dietrichlab.de/CLL_Microenvironment/) which uncovers tumour cell extrinsic influences on drug response and disease progression in CLL, and how these interactions are modulated by cell intrinsic molecular features.

Introduction

CLL is a common B-cell malignancy, attributed to the accumulation of mature B-lymphocytes in the peripheral blood, bone marrow, and lymph nodes[1]. The disease course is heterogeneous, influenced by multiple factors including B cell receptor (BCR) signalling, genetic alterations, epigenetic effects, and the tumour microenvironment[2]. Despite significant improvements to CLL treatment, including the advent of BCR inhibitors[3] and BH3-mimetics[4], CLL remains incurable. There is a compelling need to better understand cell-intrinsic and extrinsic causes of therapy failure.

The genetic landscape of CLL is well characterised. The most important features include del(17p), *TP53*-mutations, immunoglobulin heavy chain gene (IGHV) mutation status, del(13q) and trisomy 12[5,6]. This list of recurrent genetic and structural alterations has expanded in the past years[7]. The predictive value of those alterations has however declined in the context of modern targeted therapies and resistance mechanisms are incompletely understood [8].

Additionally to cell-intrinsic factors, CLL cell proliferation and survival is dependent on the lymph node microenvironment[9], which is underlined by the observation that CLL cells undergo spontaneous apoptosis *in vitro* if deprived of protective microenvironmental signals[10]. Microenvironmental stimuli can induce drug resistance *in vitro*, for example the combination of IL2 and resiquimod, a Toll-Like Receptor (TLR) 7 / 8 stimulus, induces resistance to venetoclax[11]. The CLL microenvironment constitutes a complex network of stromal and immune cells that promote cell expansion[12] via soluble factors and cell-cell contacts. Microenvironmental signalling is particularly important in protective niches, especially lymph nodes. Incomplete response to BCR inhibitors has been linked to persistent enlargement of lymph nodes[13], which are the main site of CLL proliferation[9].

89 Several studies have investigated individual components of the microenvironment in
90 leukaemia[14–18]. However, systematic studies, particularly those exploring cell-extrinsic
91 influences on drug response, are rare. Carey et al.[19] have screened acute myeloid leukaemia
92 samples with a panel of soluble factors and among them identified IL1ß as a mediator of
93 cellular expansion in Acute Myeloid Leukaemia. This example highlights the value of systematic
94 approaches to dissect tumour-microenvironment crosstalk.
95
96 Taking this approach further, we screened a panel of microenvironmental stimuli in CLL,
97 individually and in combination with drugs, and complemented our dataset with multi-omics
98 data on the patient samples. In this study, we integrate genetic, epigenetic and
99 microenvironmental modulators of drug response in CLL systematically in a large patient
100 cohort that covers the clinical and molecular diversity of CLL. Due to the dependency on
101 microenvironmental support, CLL is an important model system for the interaction between
102 malignant and microenvironmental cells in general.
103

104 **Methods**

105 **Sample preparation and drug-stimulation profiling**

106 Sample preparation, cell-culture, drug-stimulation profiling, and genomic annotation was
107 performed on 192 CLL patient samples as previously described[20] with the following
108 adjustments. Stimuli and drugs were mixed and preplated in the culture plates directly before
109 adding the cell suspensions. RPMI-1640 and supplements were acquired from Gibco by Life
110 Technologies, human serum was acquired from PAN Biotech (Cat.No. P40-2701, Lot.No:P-
111 020317). Viability was assessed by measuring ATP concentration using CellTiter-Glo
112 (Promega) after 48h. Luminescence was measured on a Perkin Elmer EnVision.

113

114 **Compounds and Stimuli**

115 Compounds and stimulatory agents were dissolved, stored, and diluted according to
116 manufacturer's protocol. HS-5 conditioned medium was produced by incubating HS-5 stromal
117 cell line to >80% confluency and cell removal by centrifugation. For a detailed list of stimuli
118 and drugs and associated concentrations, see Supp. Tables 1 and 2. Final DMSO concentration
119 did not exceed 0.3%.

120

121 **Immunohistochemistry**

122 Lymph node biopsies of CLL-infiltrated and non-neoplastic samples were formalin fixed,
123 paraffin embedded, arranged in Tissue Microarrays and stained for pSTAT6 (ab28829, Abcam)
124 and pIRAK4 (ab216513, Abcam). The slides were analysed using Qupath[21] and the
125 recommended protocol.

126

127 **Data processing and statistical analysis**

128 To quantify the responses to drugs and stimuli, we used a measure of viability relative to the
129 control, namely the natural logarithm of the ratio between CellTiter Glo luminescence readout
130 of the respective treatment and the median of luminescence readouts of the DMSO control

131 wells on the same plate, excluding controls on the outer plate edges. Data analysis was
132 performed using R version 4 and using packages including DESeq2[22], survival[23], Glmnet[24],
133 ConsensusClusterPlus[25], clusterProfiler[26], ChIPseeker[27], genomation[28] and
134 BloodCancerMultiOmics2017[29] to perform univariate association tests, multivariate regression
135 with and without lasso penalization, Cox regression, generalised linear modelling and
136 clustering. The complete analysis is described along with computer-executable transcripts at
137 github.com/Huber-group-EMBL/CLLCytokineScreen2021.
138
139 For Figure 2A, Clusters were determined by repeated hierarchical clustering over 10.000
140 repetitions with randomly selected sample subsets of 80% with the Euclidean metric using
141 ConsensusClusterPlus[25]. LDT was calculated as previously described[30]. For figure 2D
142 Multinomial regression with lasso penalisation with a matrix of genetic features (p=39), and
143 IGHV status (encoded as M = 1 and U = 0) was used to identify multivariate predictors of
144 cluster assignment. Coefficients shown are mean coefficients from 50 bootstrapped repeats
145 and error bars represent the mean ± standard deviation. Genetic features with >20% missing
146 values were excluded, and only patients with complete annotation were included in the model
147 (n=137).
148
149 Significance testing for genetic determinants of microenvironmental response shown in Figure
150 3A was performed for somatic mutations and copy number aberrations present in ≥3 patients,
151 and IGHV status (n = 54). For multivariate modelling with L1 penalisation shown in Figure 3B,
152 to generate the feature matrix genetic alterations with less than 20% missing values were
153 considered, KRAS, BRAF and NRAS mutations were summarised as RAS/RAF alterations and
154 only patient samples with complete genetic annotation were tested. In total, 39 genetic
155 features as well as IGHV status (encoded as M = 1 and U = 0), and Methylation Cluster
156 (encoded as 0, 0.5, 1) and 129 patients were included in this analysis.
157

158 For Figures 4C and D RNA-Seq data on matched samples belonging to clusters C3 and C4 were
159 selected, Ig Genes were filtered out, differentially expressed genes were calculated with the
160 design formula ~ IGHV + Cluster using the Deseq2 package and ranked based on Wald
161 statistics. GSEA was performed using the fgsea algorithm. For Fig 4E, we selected the raw
162 sequencing files from Rendeiro et al. 2016[31] to include one sample per patient passing quality
163 checks (n=52). We obtained bam files mapped to the hg19 genome and adjusted for CG bias
164 as previously outlined[32]. As trisomy 12 status was not already annotated, we called trisomy 12
165 in samples that contained > 1.4 times more reads per peak on average in chromosome 12,
166 compared to peaks on other chromosomes. We used diffTf in permutation mode[32] to infer the
167 differential TF activity between trisomy 12 and non-trisomy 12 samples using HOCOMOCO
168 v10[33] with design formula: "~ sample_processing_batch + sex + IGHV status + trisomy 12".
169 For Figures 4E and H, change in TF activity is inferred using diffTF[32], and measured as
170 weighted mean difference. For Figure 4F, we used ChIPseq data from Care et al. 2014[34] to
171 define TF targets as the closest gene to each significant ChIP peak (q value<0.05) and within
172 ±1kb of Transcription Start Site. Over-representation tests were run using clusterProfiler
173 package[26] and the method corresponds to one-sided version of Fisher's exact test. For Figure
174 4H, CLL cells have been treated for 6h hours with IBET-762 (1μM) or DMSO as solvent control
175 before isolation and transposition of DNA for ATAC Seq. Analysis of IBET-762 effects has been
176 performed as detailed above using HOCOMOCO v11. The plot depicts weighted mean
177 difference of different diffTF analyses (trisomy 12 vs. non-trisomy 12 and IBET-762 treated
178 cells vs. DMSO treated cells), absolute effect sizes should therefore not be directly compared.
179 Significantly different TFs from the trisomy 12 vs. non-trisomy 12 analysis are shown.
180
181 To generate predictor profiles for Figure 6A, linear model in Eqn. (1) was fitted in a sample -
182 specific manner, to calculate drug stimulus interaction coefficients (βint) for each patient
183 sample. Associations between the size of βint and genetic features were identified using
184 multivariate regression with L1 (lasso) regularisation with gene mutations (p = 39) and IGHV

185 status as predictors and selecting coefficients that were chosen in >90% of bootstrapped
186 model fits.
187
188 For Figure 7G+H pSTAT6 and pIRAK4 groups were defined using maximally selected rank
189 statistics based on staining intensities. The same 64 CLL lymph node samples, for which
190 survival data was available, were used for both Kaplan-Meier plots.
191
192 **Data Sharing Statement**
193 Screening data and patient annotation used in this study are available at github.com/Huber-
194 group-EMBL/CLLCytokineScreen2021. For original sequencing data and raw viability data
195 please contact the corresponding authors. We obtained CLL ATACseq data[31] from the EGA
196 (EGAD00001002110) and ChIPseq data for Spi-B binding[34] from the NCBI GEO database[35]
197 (GSE56857, GSM1370276).

198 **Results**

199 ***Ex-vivo* cell viability assay demonstrates functional diversity of cytokine and**
200 **microenvironmental signalling pathways**

201 We measured the effects of 17 cytokines and microenvironmental stimuli on cell viability in
202 192 primary CLL samples and combined each with 12 drugs to investigate the influence on
203 spontaneous and drug-induced apoptosis. (Fig 1A-C, Supp. Tables 1 -3). Viability was assessed
204 by ATP measurement after 48h and normalised to untreated controls[20].

205

206 The patient samples were characterised by DNA sequencing, mapping of copy number
207 variants, genome-wide DNA-methylation profiling, and RNA-Sequencing[20]. The distribution of
208 genetic features in our cohort is comparable to other studies (Supp. Fig 1)[6].

209

210 To assess the heterogeneity of the response patterns, we calculated Pearson correlation
211 coefficients for each pair of drugs and each pair of stimuli. For the drugs, high correlation
212 coefficients (>0.75) were associated with identical target pathways. For example, drugs
213 targeting the BCR pathway (ibrutinib, idelalisib, PRT062607 and selumetinib) were highly
214 correlated, indicating that our data sensitively and specifically reflect inter-individual
215 differences in pathway dependencies (Fig. 1D)[20].

216 In contrast, microenvironmental stimuli showed lower correlations, even where stimuli
217 targeted similar pathways (Fig. 1E, Supp. Fig. 2). For example, lower correlations were
218 observed between different stimuli of the JAK-STAT and NfκB pathways, indicating a low
219 degree of redundancy between stimuli. High correlations (R>0.75) were only seen with the
220 TLR stimuli resiquimod (TLR7/8) and CpG ODN (TLR9) as well as IL4 and IL4 + soluble CD40L
221 (sCD40L), which target near identical receptors and downstream targets.

222 Most stimuli increased CLL viability, underlining the supportive nature of the
223 microenvironment. However, IL6, tumor growth factor β (TGFβ), and TLR7/8/9 agonists in

224 IGHV-mutated (IGHV-M) samples decreased viability (Supp. Fig. 3). The strongest responses
225 were seen with IL4 and TLR7/8/9 agonists, highlighting the potency of these pathways in
226 modulating CLL survival. All screening data can be explored manually (github.com/Huber-
227 group-EMBL/CLLCytokineScreen2021) and interactively, via the shiny app
228 (www.dietrichlab.de/CLL_Microenvironment/).

229 **Patterns of responses to microenvironmental stimuli reveal two subgroups of**
230 **IGHV-M CLL with differential aggressiveness**

231 To gain a global overview over the pattern of responses to our set of microenvironmental
232 stimuli across patient samples, we clustered[25] and visualised the response profiles (Fig. 2A).

233 This analysis revealed four functionally defined subgroups with distinct response profiles. Two
234 clusters (termed C1 and C2) were enriched in IGHV-Unmutated (IGHV-U), and two in IGHV-
235 M CLL (C3 and C4). C1 and C2 showed strong responses to IL4 and TLR7/8/9 agonists. C2
236 was distinguished by stronger responses to the stimuli overall, in particular to NFκB agonists
237 including IL1β and anti-IgM. C3 responded weakly to the majority of stimuli, while C4 was
238 defined by a decreased viability upon TLR7/8/9 stimulation (Supp Fig. 4).

239 Next, we investigated whether these clusters were associated with differential *in vivo* disease
240 progression of the corresponding patients. We used lymphocyte doubling time and time to
241 next treatment to quantify the proliferative capacity of CLL cells. In line with clinical
242 observations[36], the IGHV-U enriched C1 and C2 showed a shorter lymphocyte doubling time
243 than the IGHV-M enriched C3 and C4. More strikingly, C3 showed a significantly shorter
244 lymphocyte doubling time than C4, indicating a higher proliferative capacity (Fig. 2B).
245

246 This observation was reflected in disease progression rates: The predominantly IGHV-M C3
247 showed a progression dynamic similar to the IGHV-U enriched C1 and C2. C4, however showed
248 a longer time to next treatment than C1, C2 and C3 (Cox proportional hazards model, p=

249 0.0014, <0.001, 0.005 respectively, Fig. 2C, Supp. Fig 5A&B). This points towards a subset of
250 mostly IGHV-M patients with more aggressive disease, which is characterised by its differential
251 response to microenvironmental stimuli.
252
253 To characterise genetic differences between clusters, we calculated predictor profiles for
254 cluster assignment, using multinomial regression with the sample mutation profiles (Fig. 2D).
255 IGHV status was the main predictor of all clusters. Trisomy 12 and *SF3B1* mutations were
256 associated with C2, which showed enhanced responses to many stimuli. C4, which was
257 associated with slow *in vivo* progression, showed depletion of *TP53*, *ATM*, *RAS*/*RAF* mutations
258 and gain(8q).
259
260 The observed difference in progression dynamics *in vivo* was not explained solely by the known
261 prognostic markers IGHV, trisomy 12, and *TP53*. A multivariate Cox proportional hazards
262 model accounting for these features showed an independent prognostic value of the cluster
263 assignment between C3 and C4 (p=0.039, Supp. Table 4).
264
265 To examine why C3 exhibited faster disease progression than C4, we compared baseline
266 pathway activity at the time of sampling, using RNA-Sequencing (Supp. Fig. 6A). Gene set
267 enrichment analysis revealed that key cytokine gene sets were upregulated in C3, including
268 TNFα signalling via NFκB, indicating higher pathway activity *in vivo* (Fig. 2E, Supp. Fig. 6B).
269 In addition, pathways that indicate more aggressive disease relating to proliferation,
270 metabolism and stress response were upregulated in C3 (Supp. Fig. 6 C-E).
271
272 Taken together, the patterns of responses to our set of stimuli distinguish two subgroups of
273 IGHV-M CLL (C3 and C4) that are characterised by distinct *in vivo* pathway activities and
274 differential disease progression.

275 **Microenvironmental signals and genetic features collectively determine malignant**
276 **cell survival**
277 Having observed heterogeneous responses to stimulation, we performed univariate analyses
278 of genetic determinants of stimulus response, including IGHV status, somatic gene mutations,
279 and structural variants (Fig. 3A). At least one genetic feature determined stimulus response
280 for 10/17 stimuli and at least two features for 6/17 stimuli (Student's t-tests, FDR = 10%),
281 indicating that CLL viability is controlled both by cell-intrinsic mutations and the cells'
282 microenvironment. The most prominent factors were IGHV status and trisomy 12. Responses
283 to microenvironmental stimuli were largely independent of receptor expression (Supp. Fig. 7).
284
285 To address the possible interplay of multiple genetic factors, we applied linear regression with
286 lasso regularisation to derive for each stimulus a multivariate predictor composed of genetic,
287 IGHV and DNA methylation covariates (Fig. 3B). This revealed at least one genetic predictor
288 for five of the 17 stimuli. Trisomy 12 and IGHV status were again the most common features.
289 Stimulus responses stratified by mutations, along with regression model fits can be explored
290 online (www.dietrichlab.de/CLL_Microenvironment/).
291
292 **Trisomy 12 is a key modulator of responses to stimuli**
293 Our survey of genetic determinants of stimuli response highlighted trisomy 12 as a modulator
294 of responses to IL4, TGFβ, soluble CD40L + IL4 and TLR stimuli.
295
296 TLR response has previously been shown to depend on the IGHV mutation status[16]; we
297 identified trisomy 12 as a second major determinant of response to TLR stimulation. IGHV
298 mutated CLL samples with trisomy 12 showed a strongly increased viability after TLR
299 stimulation with resiquimod compared to those without trisomy 12. IGHV unmutated CLL cells
300 showed a strong increase in viability upon TLR stimulation regardless of trisomy 12 status
301 (Fig. 4A). In line with our previous findings, we found a trend towards higher toxicity of BCR

302 inhibition in trisomy 12 patients, indicating a dependency of the trisomy 12 effect on the BCR
303 pathway (Fig. 4B)[20]. Further, we observed that the pro-survival effect of TLR stimulation, which
304 is increased in IGHV-U and trisomy 12 CLL samples, could be reversed by BCR inhibition (Supp.
305 Fig. 8)
306
307 To investigate the incompletely understood role of trisomy 12 in CLL, we investigated how it
308 might modulate responses to cell-extrinsic signals. We began by investigating the
309 transcriptomic signature of trisomy 12 and performed a gene set enrichment analysis of
310 trisomy 12 vs. non-trisomy 12 samples. Using the hallmark gene sets we found multiple
311 microenvironmental signalling cascades to be upregulated including TNFα and Interferon
312 response pathways (Fig. 4C). Since important microenvironmental pathways are missing in
313 the hallmark gene sets, we repeated this analysis for selected KEGG gene sets relating to
314 microenvironmental signalling and found the BCR and chemokine signalling pathways to be
315 upregulated (Fig. 4D). Overall, trisomy 12 CLL samples exhibit a higher activity of
316 microenvironmental signalling pathways including BCR signalling.
317
318 To investigate potential downstream effectors in trisomy 12 CLL, we visualised transcription
319 factor (TF) activity profiles based on chromatin accessibility data derived from ATAC
320 sequencing. We used the *diffTF*[32] software to identify TFs with differential binding site
321 accessibility between trisomy 12 and non-trisomy 12 CLL, using ATAC sequencing data for two
322 non-trisomy 12 and two trisomy 12 CLL PBMC samples. The binding sites of 92 TFs respectively
323 were more accessible ($p<0.05$) in the trisomy 12 samples (Supp. Fig. 9), reflecting a specific
324 signalling signature in trisomy 12 CLL. The top hit was the hematopoietic regulator Spi-B,
325 followed by PU.1, which share similar binding motifs and exhibit functional redundancy[37]. We
326 validated this finding in a second independent dataset taken from Rendeiro et al.[31], which
327 included 43 WT and nine trisomy 12 samples. The binding sites of nine TFs were more
328 accessible ($p<0.05$) in the trisomy 12 samples (Fig. 4E), and Spi-B and PU.1 were again the

329 top hits. These TFs are known to be key regulators of healthy B-cell function[38,39], controlling
330 B-cell responses to environmental cues including CD40L, TLR ligands and IL4[40].

331 We hypothesised that Spi-B might modulate proliferation by coordinating transcriptional
332 response to microenvironmental signals. To identify Spi-B target genes, we reanalysed a
333 ChIPseq dataset[34], quantifying binding in lymphoma cell lines and tested functional enrichment
334 of immune signalling pathways amongst Spi-B targets. Using selected KEGG and Reactome
335 genesets, we found that TLR, BCR and TGFβ signalling genes were enriched ($p<0.01$) amongst
336 Spi-B targets (Fig. 4F).

337 We next investigated whether Spi-B activity and the trisomy 12 signalling signature might be
338 targetable. Amongst the panel of drugs included in this screen, we noted that the
339 bromodomain inhibitor IBET-762 demonstrated higher efficacy in trisomy 12 CLL cells (Fig.
340 4G). We generated an additional ATACseq dataset consisting of four CLL PBMC samples each
341 treated with IBET-762 and DMSO as control. Using diffTF, we quantified TF binding site
342 accessibility and visualised inferred TF activity for trisomy 12 signature TFs. All nine TFs that
343 showed higher accessibility in trisomy 12 exhibited decreased accessibility upon treatment
344 with IBET-762 (Fig. 4H).

345 Taken together, we highlight trisomy 12 as a modulator of response to microenvironmental
346 signals, link these effects to differentially active BCR signalling and suggest bromodomain
347 inhibition as a possible therapeutic target in trisomy 12 patients.

348 **Mapping drug-microenvironment interactions reveals drug resistance and**
349 **sensitivity pathways**

350 Guided by the observation of reduced treatment efficacy in protective niches[13], we examined
351 the effects of the stimuli on drug response.

352 We fitted a linear model (Eqn 1) to quantify how each stimulus modulates drug efficacy beyond
353 its individual effects, such as the impact of the stimuli on baseline viability and spontaneous
354 apoptosis. β_{int}, termed the interaction factor, quantifies how the combined treatment effect
355 differs from the sum of the individual treatment effects.
356
357 $$\log V = \beta_d X_d + \beta_s X_s + \beta_{int} X_d X_s + \varepsilon \quad \text{Eqn 1}$$
358
359 V represents the viability with a given treatment, β_d, $\beta_s$and β_{int} are coefficients for the drug,
360 stimulus, and combinatorial terms respectively, $X_d$and $X_s$are indicator variables (0 or 1) for
361 the presence or absence of a drug/stimulus. ε is the vector of model residuals.
362
363 45 out of 204 combinations had a β_{int} with $p<0.05$. We classified these into four categories,
364 based on the sign of β_{int} and whether the combination effect was antagonistic or synergistic
365 (Fig. 5A-C).
366
367 Positive antagonistic interactions were the most common category, in which stimuli reversed
368 drug action and increased viability. These interactions could lead to treatment resistance *in*
369 *vivo*. They comprised known resistance mechanisms including the inactivation of ibrutinib by
370 IL4 signalling (Fig. 5D)[18], and previously unknown resistance pathways, notably the effect of
371 interferon-γ (IFNγ) signalling on ibrutinib response (Fig. 5E).
372
373 6/45 interactions were categorised as negative antagonistic, in which drug action reversed the
374 pro-survival effect of microenvironmental stimulation. These interactions point to strategies to
375 overcome treatment resistance. For instance, Pan-JAK inhibition reduced the increase in
376 viability from sCD40L + IL4 stimulation (Fig. 5F).
377

378 We observed a single positive synergistic case, whereby simultaneous treatment with IFNγ
379 and ralimetinib, a p38 MAPK inhibitor, induced a synergistic increase in viability which was not
380 observed with either single treatment (Fig. 5G), pointing towards an inhibitory effect of p38
381 activity on IFNγ signalling.
382
383 16 combinations showed negative synergistic interactions. For example, TLR9 agonist CpG
384 ODN increased the efficacy of BCR inhibition (Fig. 5H). Interestingly, in samples where TLR
385 stimulation increased viability, the addition of BCR inhibitors (ibrutinib and idelalisib)
386 suppressed this effect, indicating that the increase of viability upon TLR stimulation is
387 dependent on BCR activity. The efficacy of luminespib, a HSP90 inhibitor, increased with
388 various stimuli, including soluble anti-IgM (Fig. 5I).
389
390 Altogether, these results highlight the influence of the microenvironment on drug efficacy and
391 underline the value of microenvironmental stimulation in *ex vivo* studies of drug efficacy.
392 **Genetic features affect drug-microenvironment interactions**
393 Next, to investigate to what extent genetic driver mutations modulated the interactions
394 between stimuli and drugs, we fit the linear model in Eqn. (1) in a sample - specific manner.
395
396 This resulted in a sample-specific β_{int} interaction coefficient for each drug - stimulus
397 combination. We looked for associations between the size of β_{int} and genetic features using
398 multivariate regression with L1 (lasso) regularisation, with gene mutations and IGHV status as
399 predictors. We generated a predictor profile for each drug - stimulus combination, considering
400 predictors that were selected in >90% of bootstrapped model fits. In total, we found genetic
401 modulators for 60/204 interactions (Fig 6A, Supp Fig. 10). Trisomy 12 and IGHV status
402 modulated the largest number of interactions.
403

404 For example, we found the value of β_{int} for fludarabine and CpG ODN to be modulated by six
405 genetic factors; most strongly by IGHV status, del(11q), and trisomy 12 (Fig. 6B).
406 In IGHV-M non-trisomy 12 samples, fludarabine efficacy increased in the presence of TLR
407 stimulation, whilst in the other subgroups TLR stimulation induced resistance to fludarabine
408 (Fig. 6C).
409
410 Our approach also identified interactions dependent on single treatment effects. IL4 induced
411 complete resistance to ibrutinib regardless of higher ibrutinib efficacy in trisomy 12 and IGHV-
412 U samples. This highlights the breadth of IL4-induced resistance to ibrutinib in CLL across
413 genetic backgrounds (Fig. 6D, Supp. Fig. 11).
414
415 Overall, these findings illustrate how the presence of known genetic alterations determines
416 how drugs and external stimuli interact with each other.
417 **The key resistance pathways IL4 and TLR show increased activity in CLL-infiltrated**
418 **lymph nodes**
419
420 Microenvironmental signalling within lymph nodes has been implicated in treatment
421 resistance[9,41–43], though a clear understanding of the mechanisms involved remains missing.
422 Since IL4 and TLR signalling were the most prominent modulators of drug response in our
423 study, we assessed their activity within the lymph node niche. We stained paraffin embedded
424 sections of 100 CLL-infiltrated and 100 non-neoplastic lymph nodes for pSTAT6, an essential
425 downstream target of IL4 (Supp. Fig. 12), and pIRAK4, a downstream target of TLR7/8/9.
426
427 The CLL-infiltrated lymph nodes showed higher levels of pSTAT6 (Fig. 7A) and pIRAK4 (Fig.
428 7B). Examples are shown in Fig. 7C-F.
429

430 To investigate the influence of microenvironmental activity in lymph nodes on CLL disease
431 progression, we correlated staining intensity to time to next treatment. High activity of pSTAT-
432 6 correlated with shorter time to next treatment (Fig. 7G), the same trend could be observed
433 with higher pIRAK4 (Fig. 7H). Higher IL4 activity within the lymph node appeared to relate to
434 shorter time to next treatment, and may provide further evidence to the hypothesis that
435 microenvironmental activity promotes treatment resistance within the lymph node, eventually
436 leading to relapse.

437 **Discussion**

438 Our work maps the effects of microenvironmental stimuli in the presence of drugs and links
439 these to underlying molecular properties across 192 primary CLL samples. We employ all
440 combinations of 17 stimuli with 12 drugs as a reductionist model of microenvironmental
441 signalling. We account for the confounding effects of spontaneous apoptosis *ex vivo* and
442 dissect the effect of individual microenvironmental stimuli on baseline viability and drug
443 toxicity. The results may serve as building blocks for a more holistic understanding of the
444 interactions of tumour genetics, microenvironment, and drug response in complex *in vivo*
445 situations.

446 We discover that CLL subgroups can be extracted from microenvironmental response
447 phenotypes and that this classification is linked to distinct molecular profiles and clinical
448 outcomes. IGHV-M samples with weaker responses to microenvironmental stimuli showed
449 faster disease progression, highlighting the important role microenvironmental signalling may
450 play in CLL pathophysiology.

451 The sensitivity afforded by our approach enabled us to identify drug-stimulus interactions,
452 meaning instances where the effect of a drug on the tumour cells is modulated by a
453 microenvironmental stimulus. Our assay recapitulated known drug-resistance phenomena,
454 such as the impact of IL4 stimulation on ibrutinib and idelalisib[18] and identified new ones,
455 including IFNγ-induced resistance to BCR inhibition. Systematic mapping of drug-stimulus
456 interactions, such as generated in this study, can be used to inform biology-based
457 combinatorial treatments across different entities.

458 We demonstrated the breadth of IL4-induced resistance against kinase inhibitors and
459 chemotherapeutics across a range of genetic backgrounds. IL4 induced complete resistance
460 to BCR inhibitors across genetic subgroups, despite greater BCR inhibitor efficacy in IGHV-U
461 CLL. Further, we observed increased IL4 activity within CLL-infiltrated lymph nodes and the
462 association of higher activity with faster disease progression. Our work highlights the

463 significance of IL4 within the lymph node niche, especially since proliferation[9] and resistance
464 to BCR inhibition[13] is linked to lymph nodes and our recent work suggests T follicular helper
465 cells as a source of IL4[44]. Targeting pathways downstream of IL4, via JAK inhibition, has been
466 reported to improve BCR response in non-responding CLL patients[45].

467 Underneath cell-extrinsic factors that control the apoptotic and proliferative activity of tumour
468 cells in response to drugs there lies the network of cell-intrinsic molecular components. We
469 used multivariate modelling to capture the impact of molecular features on responses to stimuli
470 and drugs. For instance, the response to TLR stimulation depended on IGHV status, trisomy
471 12, del11q, del13q and ATM, reflecting the multiple layers of biology involved. Most strikingly,
472 we observed that TLR stimulation increased fludarabine toxicity in the subgroup of IGHV-M
473 non-trisomy 12 patient samples, while it led to fludarabine resistance in all other backgrounds.
474 This finding combined with our observation that TLR signalling is highly active in CLL-infiltrated
475 lymph nodes might help explain the heterogeneous effects of chemotherapy in CLL, in
476 particular that fludarabine therapy can achieve lasting remission in IGHV-M but not in IGHV-
477 U patients.
478
479 Beyond TLR, trisomy 12 modulated a broad range of stimulus responses and drug-stimulus
480 interactions, comparable to the impact of IGHV status. Molecularly, we link the observed
481 trisomy 12 phenotype to upregulated microenvironmental signalling and higher activity of Spi-
482 B, an essential regulator of environmental sensing in B-cells[40]. The TF signature associated
483 with trisomy 12 can be reversed by bromodomain inhibition and trisomy 12 samples exhibit
484 increased sensitivity to bromodomain inhibition, indicating this as potential therapeutic
485 strategy in trisomy 12 CLL.
486
487 We present a data resource for the study of drug response in the context of cell-intrinsic and
488 cell-extrinsic modulators. The data may inform targeted mechanistic investigations[30] and direct

489 efforts for combination therapies. The entire dataset, including the reproducible analysis, can
490 be downloaded from the online repository (github.com/Huber-group-
491 EMBL/CLLCytokineScreen2021), or explored interactively
492 (www.dietrichlab.de/CLL_Microenvironment/).

493 **Acknowledgments**

494 We thank the Department of Medicine V, University of Heidelberg, Molecular Medicine
495 Partnership Unit (MMPU), EMBL Heidelberg and DKFZ/Heidelberg Center for Personalized
496 Oncology (DKFZ/HIPO) for technical support and funding. H.A.R.G. was supported by a
497 Joachim-Herz Add-on Fellowship for Interdisciplinary Science. P.M.B was supported by a
498 doctoral scholarship of the Franziska-Kolb foundation. S.D. was supported by the Else Kröner
499 Fresenius Foundation, the Federal Ministry of Education and Research (SYMPATHY) and the
500 German Research Foundation (SFB873). J.L., S.D. and W.H. were supported by the German
501 Federal Ministry of Education and Research (CompLS project MOFA under grant agreement
502 number 031L0171A). T.R. was supported by a physician scientist fellowship of the Medical
503 Faculty of University Heidelberg and the German Federal Ministry of Education and Research
504 (CompLS project SIMONA under grant agreement number 031L0263A). For experimental
505 technical support and expertise, we thank Mareike Knoll, Angela Lenze, Brian Lai, and Vladimir
506 Benes, and Nayara Trevisan Doimo de Azevedohe of the EMBL Genomics Core Facility. We
507 thank EMBL's IT Services for providing data management and computing infrastructure and
508 Simone Bell for organisational support. We thank Mike Smith and Frederik Ziebell for advice
509 on statistics and analysis, Martina Seiffert for the HS-5 stromal cell line, and Michael Boutros,
510 Moritz Gerstung, Nassos Typas, and Simon Anders for their comments on the manuscript and
511 their valued advice.

512 P.M.B is a MD candidate at the University of Heidelberg. This work is submitted in partial
513 fulfilment of the requirement for the MD. H.A.R.G is a PhD candidate for the joint PhD degree
514 between EMBL and Heidelberg University, Faculty of Biosciences. This work is submitted in
515 partial fulfilment of the requirement for the PhD.

516 **Author contributions**

517 S.D. and P.M.B. designed the experiments. S.D., W.H., H.A.R.G., and P.M.B. conceptualised
518 the data analysis. W.H. and S.D. supervised the study. W.H., T.Z. and S.D. conceptualised the
519 multi-omics approach to analyse CLL drug response. P.M.B. performed the drug-stimulus
520 profiling experiments with support from C.K., S.S., and L.W.. T.Z., C.M.T., and P.D. provided
521 guidance on experimental protocols. H.A.R.G., P.M.B, J.H., J.L., S.D. performed data
522 processing and curation. H.A.R.G., and P.M.B. analysed and interpreted the data, with support
523 from W.H., S.D., J.L, S.H., and T.R., and produced the figures with input from W.H. and S.D..
524 H.A.R.G. performed statistical inference and regression modelling, P.M.B. performed
525 exploratory analysis and integration with clinical data. T.B. and S.H. performed the shRNA
526 knockdown experiments, J.B.Z. and I.B. provided the ATACseq dataset used in Figure 4 and
527 quantified differential transcription factor activity, M.K., K.K., and C.Z. generated the
528 immunohistochemistry data, and P.M.B. analysed these data. H.A.R.G. designed and wrote
529 the Shiny app and the software documentation. P.M.B. and H.A.R.G. wrote the manuscript,
530 with input from S.D. and W.H.. All authors reviewed and edited the manuscript.

531

532 **Conflict of Interest Disclosures**

533 The authors declare that they have no conflict of interests.

534

535 **References**

536 1. Fabbri, G. & Dalla-Favera, R. The molecular pathogenesis of chronic lymphocytic
537 leukaemia. *Nat. Rev. Cancer* **16**, 145–162 (2016).
538 2. Puente, X. S., Jares, P. & Campo, E. Chronic lymphocytic leukemia and mantle cell
539 lymphoma: crossroads of genetic and microenvironment interactions. *Blood* **131**, 2283–
540 2296 (2018).
541 3. Burger, J. A. *et al.* Ibrutinib as Initial Therapy for Patients with Chronic Lymphocytic

542 Leukemia. *N. Engl. J. Med.* **373**, 2425–2437 (2015).
543 4. Fischer, K. *et al.* Venetoclax and Obinutuzumab in Patients with CLL and Coexisting
544 Conditions. *N. Engl. J. Med.* **380**, 2225–2236 (2019).
545 5. Gaidano, G. & Rossi, D. The mutational landscape of chronic lymphocytic leukemia and
546 its impact on prognosis and treatment. *Hematology Am. Soc. Hematol. Educ. Program*
547 **2017**, 329–337 (2017).
548 6. Döhner, H. *et al.* Genomic aberrations and survival in chronic lymphocytic leukemia. *N.*
549 *Engl. J. Med.* **343**, 1910–1916 (2000).
550 7. Strefford, J. C. The genomic landscape of chronic lymphocytic leukaemia: biological and
551 clinical implications. *Br. J. Haematol.* **169**, 14–31 (2015).
552 8. Burger, J. A. *et al.* Long-term efficacy and safety of first-line ibrutinib treatment for
553 patients with CLL/SLL: 5 years of follow-up from the phase 3 RESONATE-2 study.
554 *Leukemia* **34**, 787–798 (2020).
555 9. Herndon, T. M. *et al.* Direct in vivo evidence for increased proliferation of CLL cells in
556 lymph nodes compared to bone marrow and peripheral blood. *Leukemia* **31**, 1340–1347
557 (2017).
558 10. Collins, R. J. *et al.* Spontaneous programmed death (apoptosis) of B-chronic lymphocytic
559 leukaemia cells following their culture in vitro. *Br. J. Haematol.* **71**, 343–350 (1989).
560 11. Oppermann, S. *et al.* High-content screening identifies kinase inhibitors that overcome
561 venetoclax resistance in activated CLL cells. *Blood* **128**, 934–947 (2016).
562 12. Ten Hacken, E. & Burger, J. A. Microenvironment interactions and B-cell receptor
563 signaling in Chronic Lymphocytic Leukemia: Implications for disease pathogenesis and
564 treatment. *Biochim. Biophys. Acta* **1863**, 401–413 (2016).
565 13. Ahn, I. E. *et al.* Depth and durability of response to ibrutinib in CLL: 5-year follow-up of
566 a phase 2 study. *Blood* **131**, 2357–2366 (2018).
567 14. Chen, Z. *et al.* LINKING MICROENVIRONMENTAL SIGNALS TO METABOLIC SWITCHES
568 AND IBRUTINIB RESPONSE IN CHRONIC LYMPHOCYTIC LEUKEMIA: PS1125.

569 *HemaSphere* **3**, 509–510 (2019).
570 15. Jayappa, K. D. *et al.* Microenvironmental agonists generate phenotypic resistance to
571 combined ibrutinib plus venetoclax in CLL and MCL. *Blood Adv* **1**, 933–946 (2017).
572 16. Chatzouli, M. *et al.* Heterogeneous functional effects of concomitant B cell receptor and
573 TLR stimulation in chronic lymphocytic leukemia with mutated versus unmutated Ig
574 genes. *J. Immunol.* **192**, 4518–4524 (2014).
575 17. Dietrich, S. *et al.* Leflunomide induces apoptosis in fludarabine-resistant and clinically
576 refractory CLL cells. *Clin. Cancer Res.* **18**, 417–431 (2012).
577 18. Aguilar-Hernandez, M. M. *et al.* IL-4 enhances expression and function of surface IgM in
578 CLL cells. *Blood* **127**, 3015–3025 (2016).
579 19. Carey, A. *et al.* Identification of Interleukin-1 by Functional Screening as a Key Mediator
580 of Cellular Expansion and Disease Progression in Acute Myeloid Leukemia. *Cell Rep.* **18**,
581 3204–3218 (2017).
582 20. Dietrich, S. *et al.* Drug-perturbation-based stratification of blood cancer. *J. Clin. Invest.*
583 **128**, 427–445 (2018).
584 21. Bankhead, P. *et al.* QuPath: Open source software for digital pathology image analysis.
585 *Sci. Rep.* **7**, 1–7 (2017).
586 22. Love, M. I., Huber, W. & Anders, S. Moderated estimation of fold change and dispersion
587 for RNA-seq data with DESeq2. *Genome Biol.* **15**, 550 (2014).
588 23. Therneau, T. M. & Grambsch, P. M. *Modeling Survival Data: Extending the Cox Model*.
589 (Springer Science & Business Media, 2000).
590 24. Friedman, J., Hastie, T. & Tibshirani, R. Regularization Paths for Generalized Linear
591 Models via Coordinate Descent. *J. Stat. Softw.* **33**, 1–22 (2010).
592 25. Wilkerson, M. D. & Hayes, D. N. ConsensusClusterPlus: a class discovery tool with
593 confidence assessments and item tracking. *Bioinformatics* **26**, 1572–1573 (2010).
594 26. Yu, G., Wang, L.-G., Han, Y. & He, Q.-Y. clusterProfiler: an R Package for Comparing
595 Biological Themes Among Gene Clusters. *OMICS: A Journal of Integrative Biology* vol.

596 16 284–287 (2012).
597 27. Yu, G., Wang, L.-G. & He, Q.-Y. ChIPseeker: an R/Bioconductor package for ChIP peak
598 annotation, comparison and visualization. *Bioinformatics* **31**, 2382–2383 (2015).
599 28. Akalin, A., Franke, V., Vlahoviček, K., Mason, C. E. & Schübeler, D. Genomation: a
600 toolkit to summarize, annotate and visualize genomic intervals. *Bioinformatics* **31**,
601 1127–1129 (2015).
602 29. Malgorzata Oles, Sascha Dietrich, Junyan Lu, Britta Velten, Andreas Mock, Vladislav Kim,
603 Wolfgang Huber. *BloodCancerMultiOmics2017*. (Bioconductor, 2018).
604 doi:10.18129/B9.BIOC.BLOODCANCERMULTIOMICS2017.
605 30. Lu, J. *et al.* Multi-omics reveals clinically relevant proliferative drive associated with
606 mTOR-MYC-OXPHOS activity in chronic lymphocytic leukemia. *Nat Cancer* (2021)
607 doi:10.1038/s43018-021-00216-6.
608 31. Rendeiro, A. F. *et al.* Chromatin accessibility maps of chronic lymphocytic leukaemia
609 identify subtype-specific epigenome signatures and transcription regulatory networks.
610 *Nat. Commun.* **7**, 11938 (2016).
611 32. Berest, I. *et al.* Quantification of Differential Transcription Factor Activity and
612 Multiomics-Based Classification into Activators and Repressors: diffTF. *Cell Rep.* **29**,
613 3147–3159.e12 (2019).
614 33. Kulakovskiy, I. V. *et al.* HOCOMOCO: expansion and enhancement of the collection of
615 transcription factor binding sites models. *Nucleic Acids Res.* **44**, D116–25 (2016).
616 34. Care, M. A. *et al.* SPIB and BATF provide alternate determinants of IRF4 occupancy in
617 diffuse large B-cell lymphoma linked to disease heterogeneity. *Nucleic Acids Res.* **42**,
618 7591–7610 (2014).
619 35. Edgar, R., Domrachev, M. & Lash, A. E. Gene Expression Omnibus: NCBI gene
620 expression and hybridization array data repository. *Nucleic Acids Res.* **30**, 207–210
621 (2002).
622 36. Baumann, T. *et al.* Lymphocyte doubling time in chronic lymphocytic leukemia modern

era: a real-life study in 848 unselected patients. *Leukemia* (2021) doi:10.1038/s41375-021-01149-w.

37. Garrett-Sinha, L. A., Dahl, R., Rao, S., Barton, K. P. & Simon, M. C. PU.1 exhibits partial functional redundancy with Spi-B, but not with Ets-1 or Elf-1. *Blood* **97**, 2908–2912 (2001).
38. Turkistany, S. A. & DeKoter, R. P. The Transcription Factor PU.1 is a Critical Regulator of Cellular Communication in the Immune System. *Arch. Immunol. Ther. Exp.* **59**, 431–440 (2011).
39. Ray-Gallet, D., Mao, C., Tavitian, A. & Moreau-Gachelin, F. DNA binding specificities of Spi-1/PU.1 and Spi-B transcription factors and identification of a Spi-1/Spi-B binding site in the c-fes/c-fps promoter. *Oncogene* **11**, 303–313 (1995).
40. Willis, S. N. *et al.* Environmental sensing by mature B cells is controlled by the transcription factors PU.1 and SpiB. *Nat. Commun.* **8**, 1426 (2017).
41. Hayden, R. E., Pratt, G., Roberts, C., Drayson, M. T. & Bunce, C. M. Treatment of chronic lymphocytic leukemia requires targeting of the protective lymph node environment with novel therapeutic approaches. *Leuk. Lymphoma* **53**, 537–549 (2012).
42. Mittal, A. K. *et al.* Chronic lymphocytic leukemia cells in a lymph node microenvironment depict molecular signature associated with an aggressive disease. *Mol. Med.* **20**, 290–301 (2014).
43. Yan, X.-J. *et al.* Identification of outcome-correlated cytokine clusters in chronic lymphocytic leukemia. *Blood* **118**, 5201–5210 (2011).
44. Roider, T. *et al.* Dissecting intratumour heterogeneity of nodal B-cell lymphomas at the transcriptional, genetic and drug-response levels. *Nature Cell Biology* vol. 22 896–906 (2020).
45. Spaner, D. E., McCaw, L., Wang, G., Tsui, H. & Shi, Y. Persistent janus kinase-signaling in chronic lymphocytic leukemia patients on ibrutinib: Results of a phase I trial. *Cancer Med.* **8**, 1540–1550 (2019).

Figure 1

A

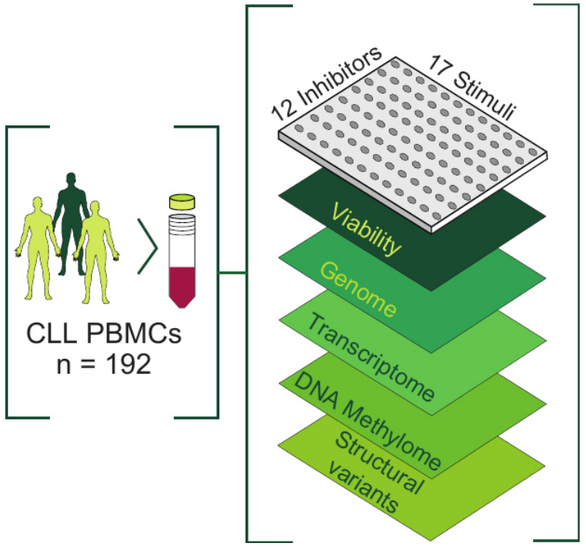

B

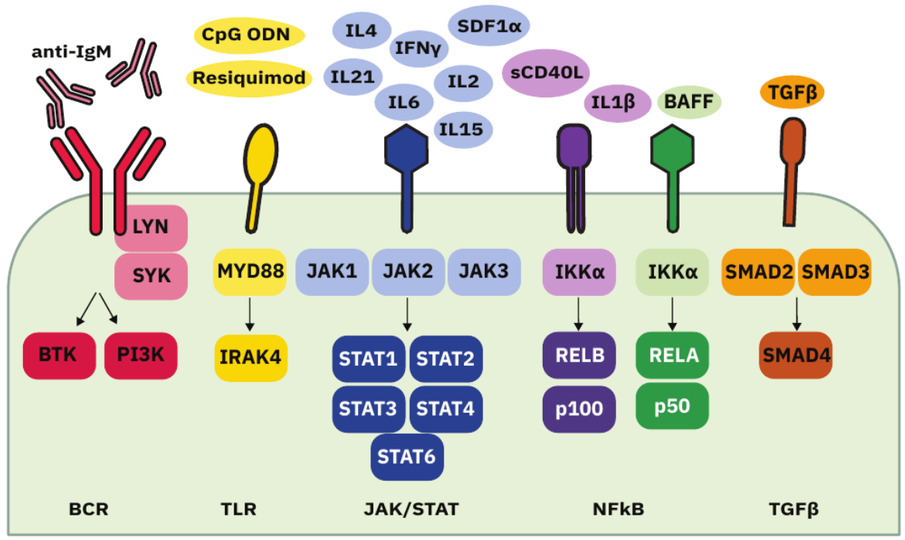

C

Drug	Target	Category
Ibrutinib	BTK	BCR
Idelalisib	PI3K delta	BCR
PRT062607	SYK	BCR
Fludarabine	Purine analogue	DDR
Nutlin-3a	MDM2	DDR
I-BET 762	BRD2/3/4	Epigenome
Luminespib	HSP90	HSP90
Pyridone-6	JAK1/2/3	JAK/STAT
Selumetinib	MEK1/2	MAPK
Ralimetinib	p38 MAPK	MAPK
Everolimus	mTOR	mTOR
BAY-11-7085	NFkB	NFkB

D

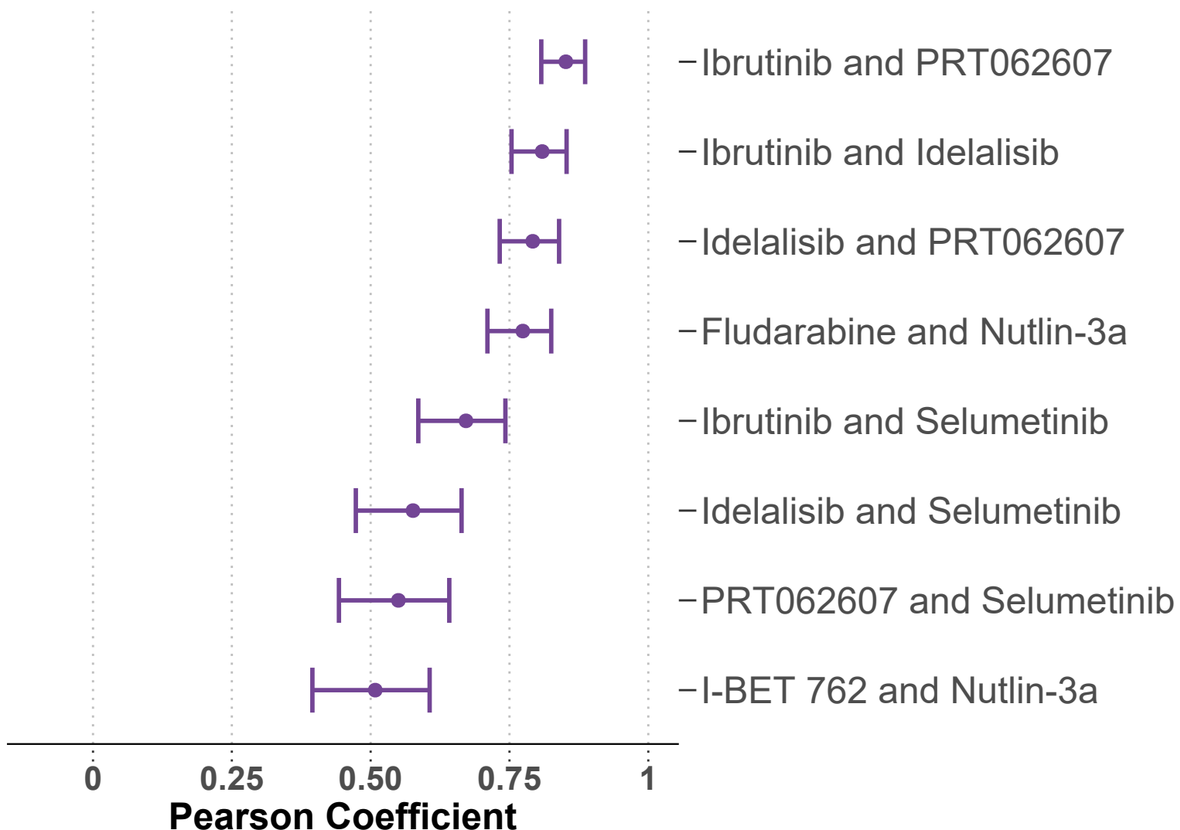

E

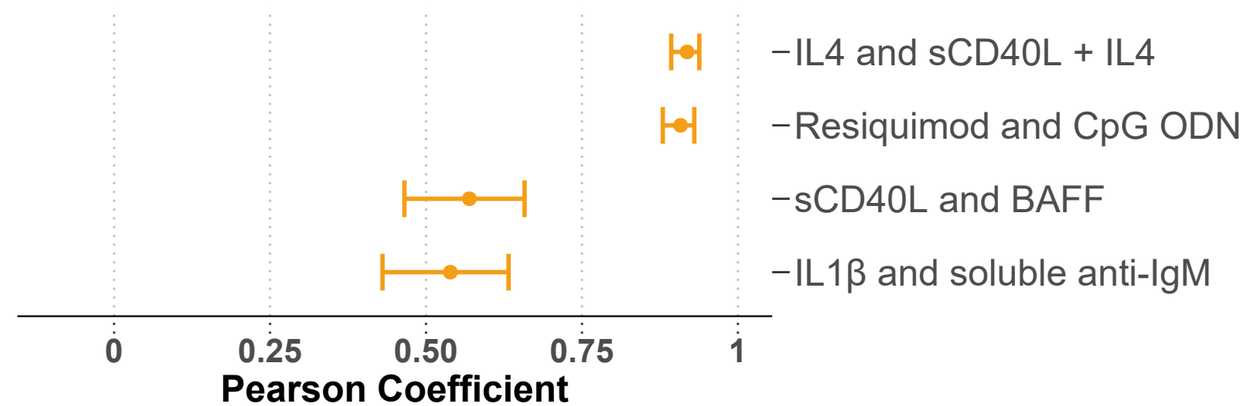

F

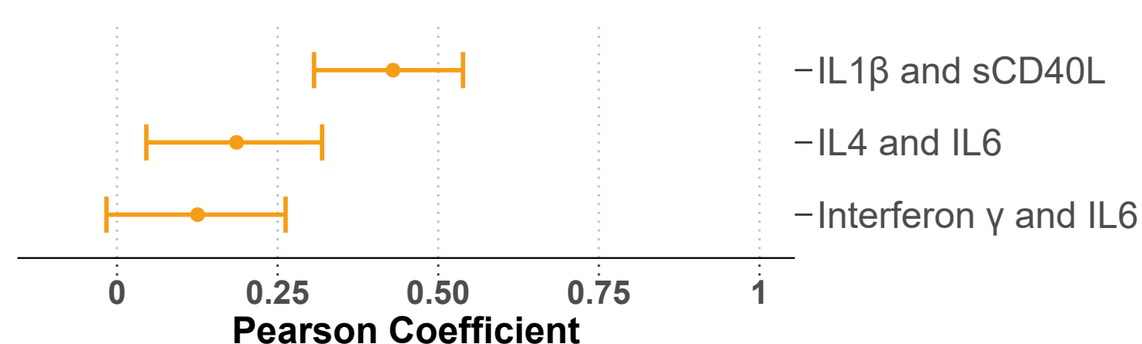

Figure 1. Study outline and overview of drugs and stimuli.

(A) Schematic of experimental protocol. By combining 12 drugs and 17 stimuli, we systematically queried the effects of simultaneous stimulation and inhibition of critical pathways in CLL (n=192). Integrating functional drug-stimulus response profiling with four additional omics layers, we identified pro-survival pathways, underlying molecular modulators of drug and microenvironment responses, and drug-stimulus interactions in CLL. All screening data can be explored either manually (github.com/Huber-group-EMBL/CLLCytokineScreen2021) or interactively, via the shiny app (www.dietrichlab.de/CLL_Microenvironment/).

(B) Overview of stimuli included in the screen and summary of their associated targets. HS-5 conditioned medium is omitted, as no specific target can be shown.

(C) Table of drugs included in the screen. Drug target, and category of target are also shown.

(D - F) Pearson correlation coefficients of drug-drug and stimulus-stimulus correlations. (D) and (E) show highest drug -drug and stimulus-stimulus correlations, (F) shows selected combinations of stimuli targeting the NfKB and JAK-STAT pathways as examples of stimuli which share very similar receptors and downstream target profiles but show a divergence of effects.

Figure 2

A

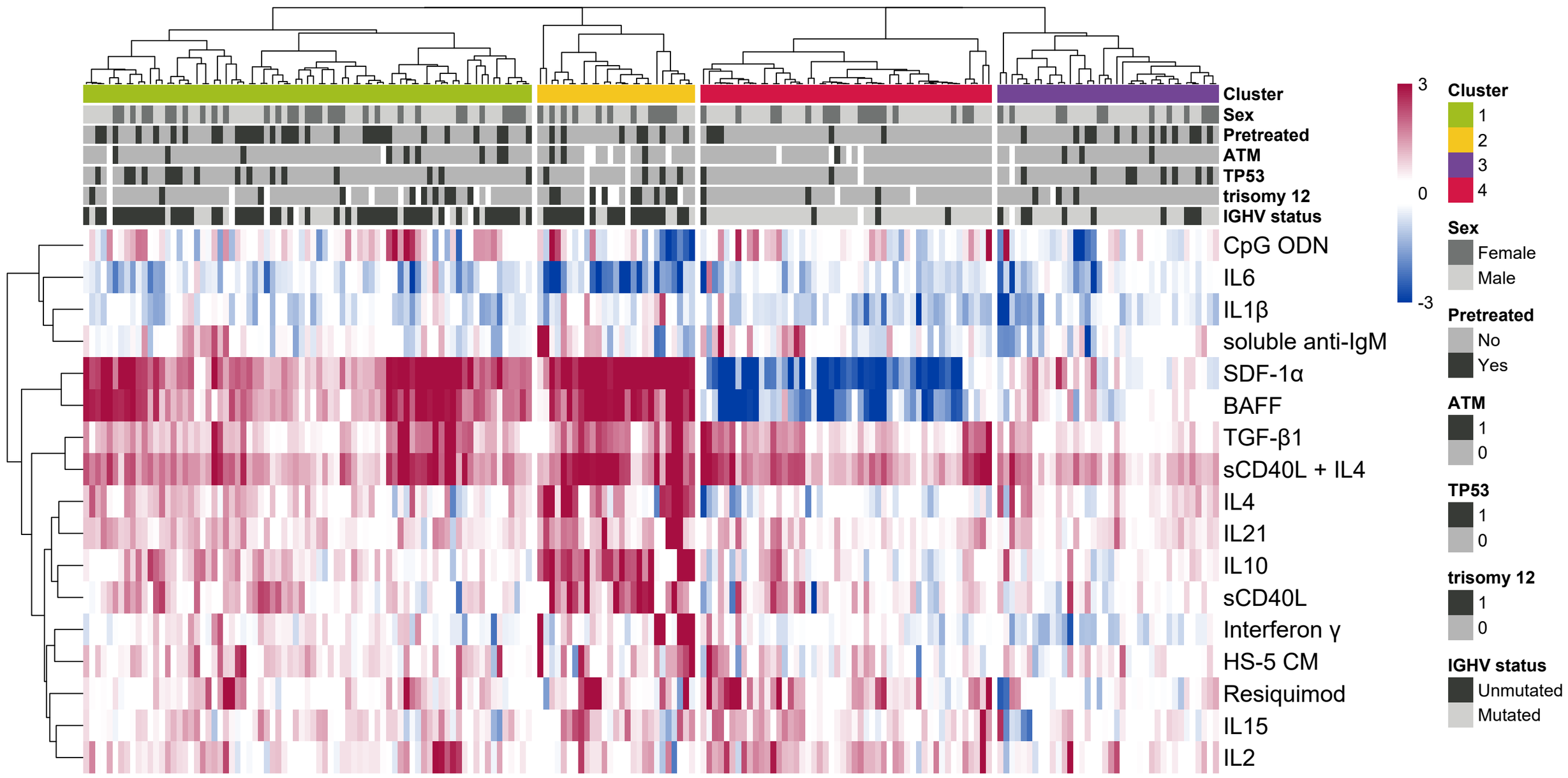

B

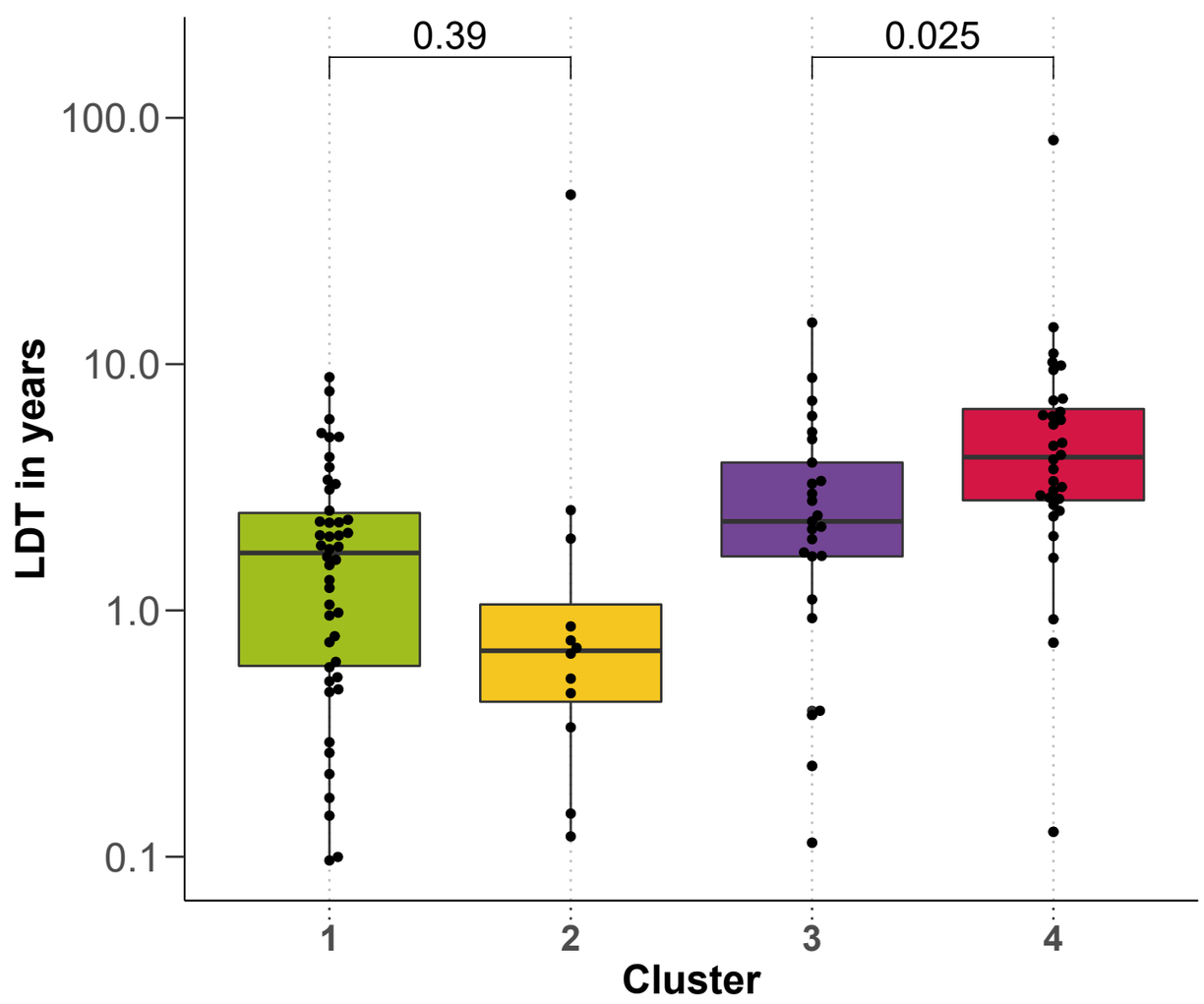

C

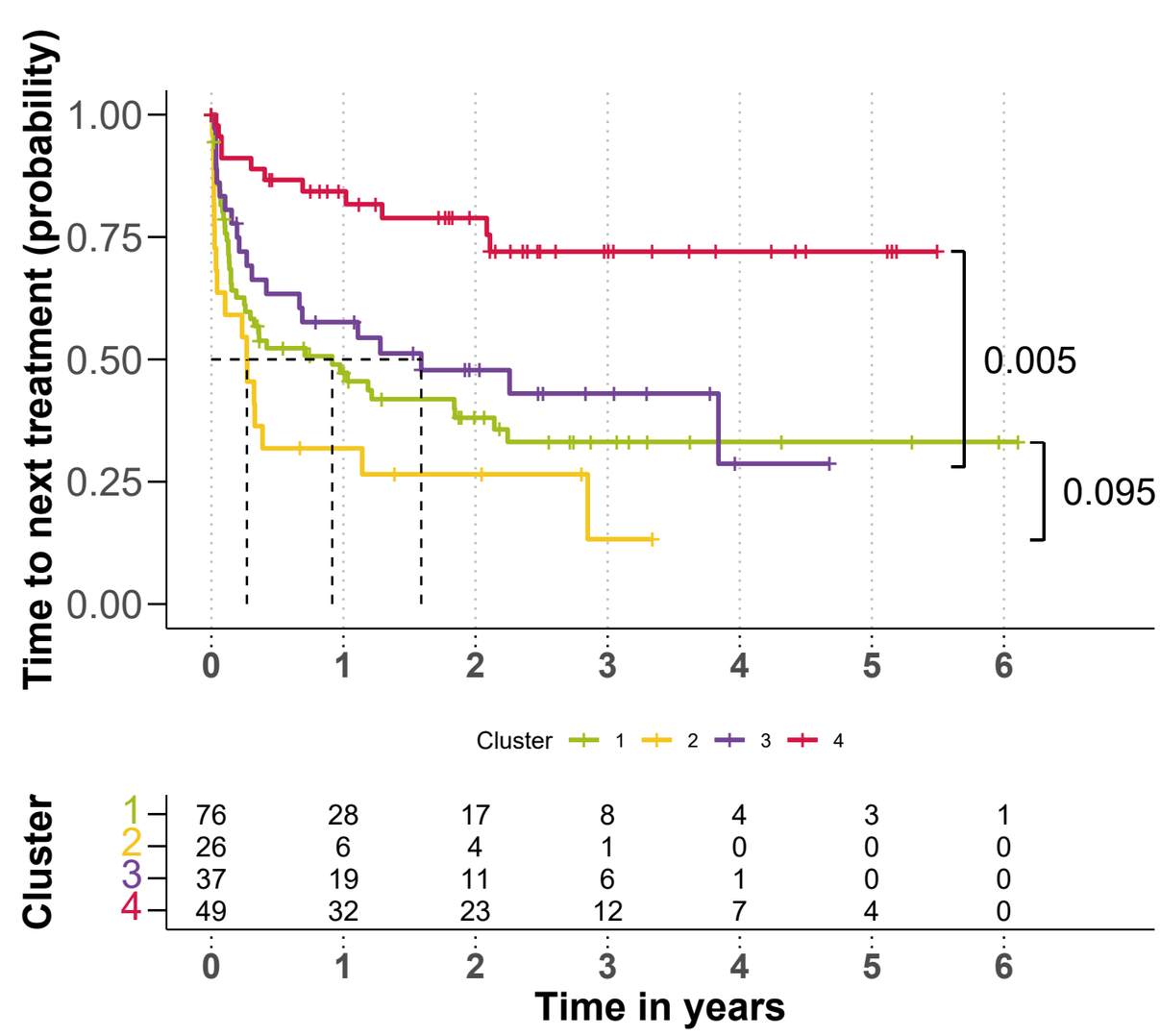

D

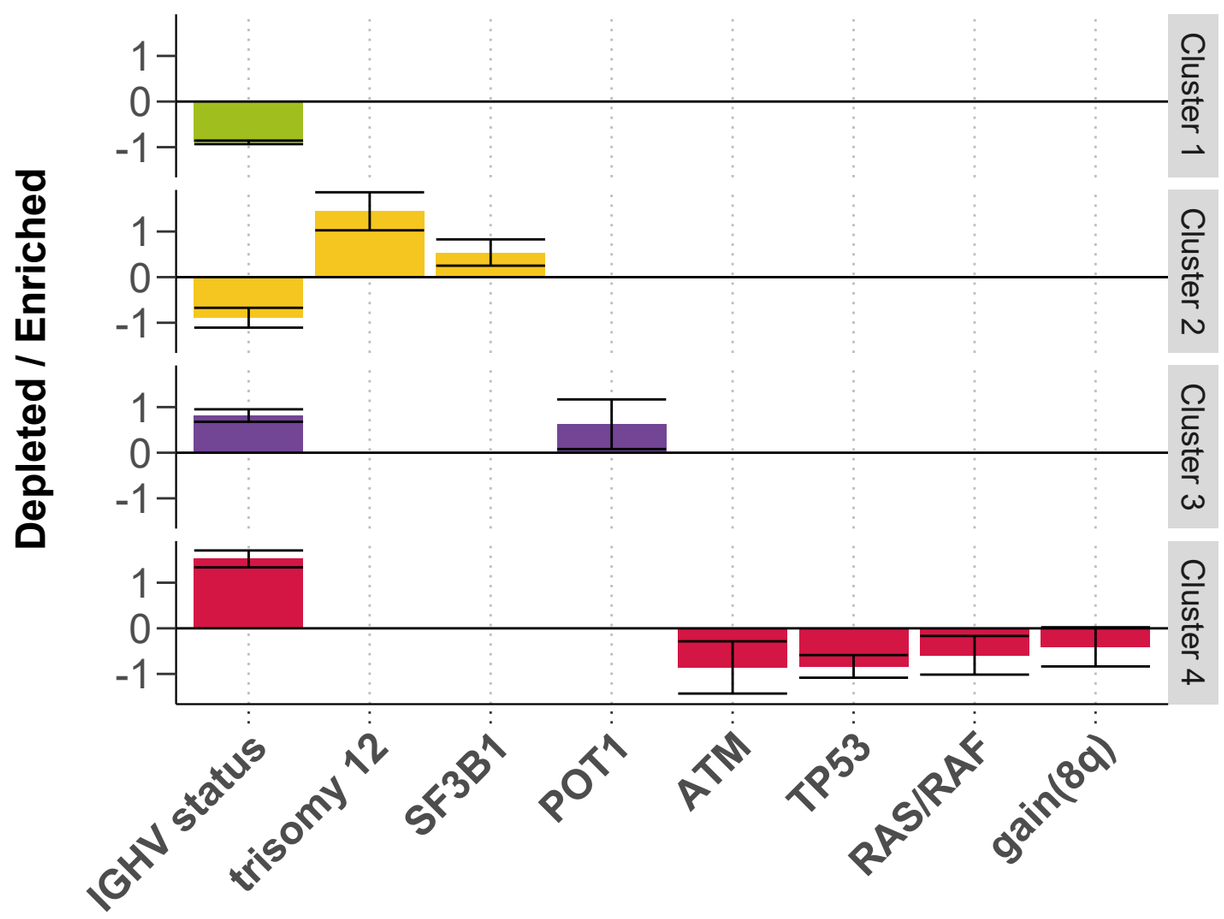

E

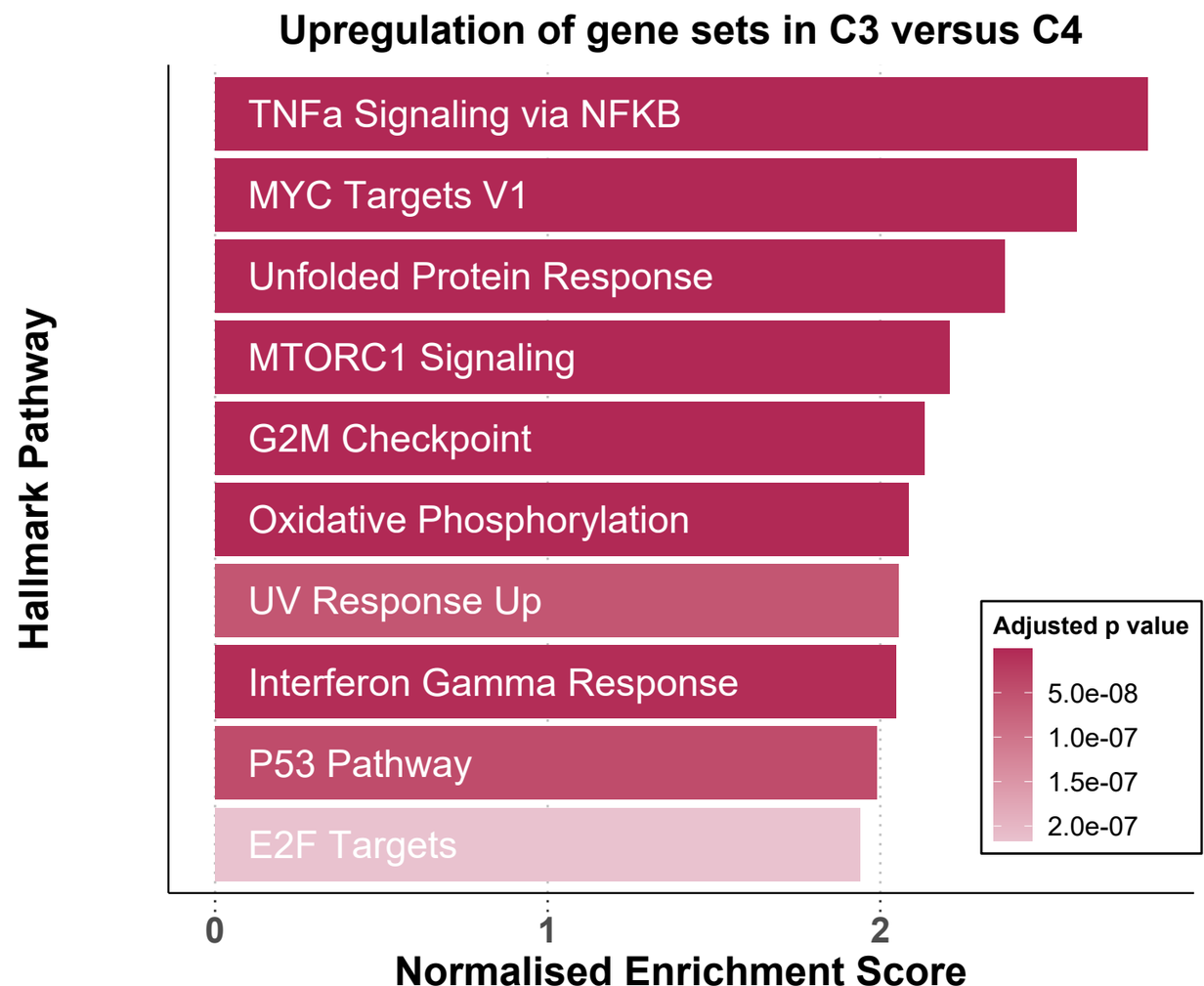

Figure 2. Ex vivo microenvironmental response profiling reveals subgroups with distinct molecular profiles and disease progression.

(A) Heatmap showing the viability after treatment with microenvironmental stimuli. Rows represent microenvironmental stimuli and columns represent primary CLL samples, annotated for their genetic background, sex and pre-treatment status above. Red values indicate increased viability upon treatment, blue indicates decreased viability. Data is row-scaled.

(B) Lymphocyte doubling time, a clinical marker for disease progression, plotted for each cluster. P-values from Student's t-tests.

(C) Kaplan-Meier curves of time to next treatment for each cluster. P-values from univariate Cox proportional hazard models comparing IGHV-U enriched C1 with C2, and IGHV-M enriched C3 with C4.

(D) Multinomial regression with lasso penalisation to identify enrichment or depletion of genetic features within each cluster.

(E) Gene set enrichment analysis (GSEA) comparing on expression of genes in samples from C3 and C4. Normalised enrichment scores are shown for top 10 most significant pathways upregulated in C3 versus C4.

Figure 3

A

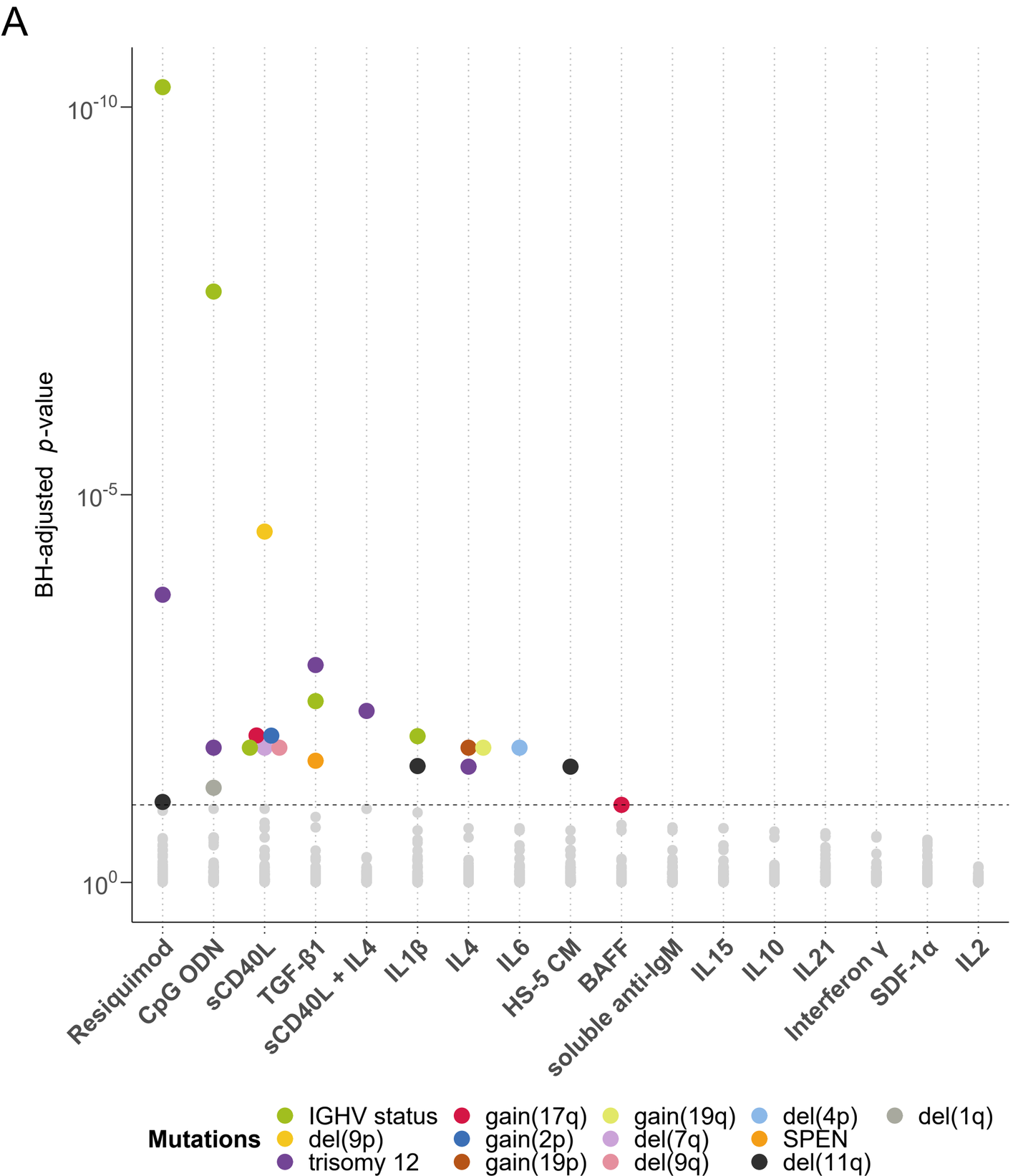
BH-adjusted p-value
10^-10
10^-5
10^0
Resiquimod
CpG ODN
sCD40L
TGF-β1
sCD40L + IL4
IL1β
IL4
IL6
HS-5 CM
BAFF
soluble anti-IgM
IL15
IL10
IL21
Interferon γ
SDF-1α
IL2
Mutations
IGHV status
del(9p)
trisomy 12
gain(17q)
gain(2p)
gain(19p)
gain(19q)
del(7q)
del(9q)
del(4p)
SPEN
del(11q)
del(1q)

B

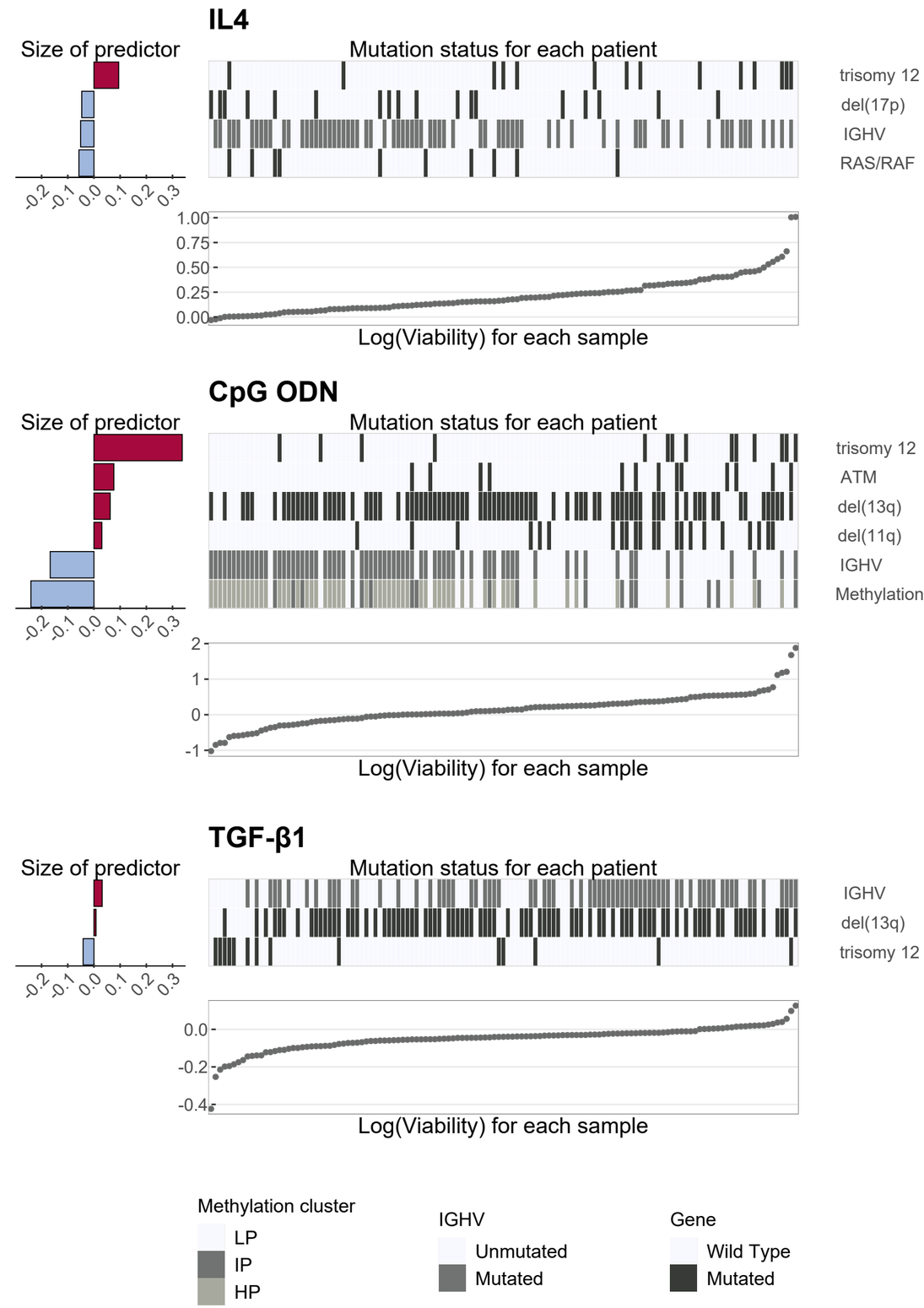
IL4
Size of predictor
Mutation status for each patient
trisomy 12
del(17p)
IGHV
RAS/RAF
Log(Viability) for each sample
CpG ODN
Size of predictor
Mutation status for each patient
trisomy 12
ATM
del(13q)
del(11q)
IGHV
Methylation
Log(Viability) for each sample
TGF-β1
Size of predictor
Mutation status for each patient
IGHV
del(13q)
trisomy 12
Log(Viability) for each sample
Methylation cluster
LP
IP
HP
IGHV
Unmutated
Mutated
Gene
Wild Type
Mutated

Figure 3. Responses to microenvironmental signals are modulated by genetic alterations recurrent in CLL.

(A) Overview of results of all tested gene - stimulus associations. x-axis shows stimuli, y-axis shows p-values from Student's t-test (two-sided, with equal variance). Each dot represents a gene-stimulus association. Tests with p-values smaller than the threshold corresponding to a false discovery rate (FDR) of 10% (method of Benjamini and Hochberg) are indicated by coloured circles, where the colours represent the gene mutations and structural aberrations.

(B) Predictor profiles for selected stimuli to represent gene - stimulus associations identified through Gaussian linear modelling with L1-penalty. Within the plots, the bar plots on the left indicate size and sign of coefficients assigned to the named predictors. Positive coefficients indicate higher viability after stimulation if the feature is present. Scatter plots indicate log(viability) values, in order of magnitude, for each individual sample. Heatmaps show mutation status for each of the genetic predictors for the corresponding samples in the scatter plot.

Figure 4

A

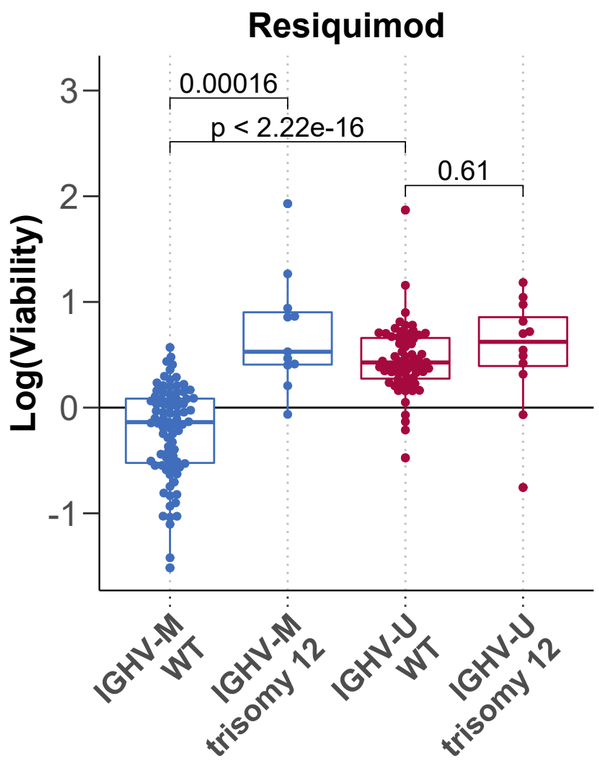

B

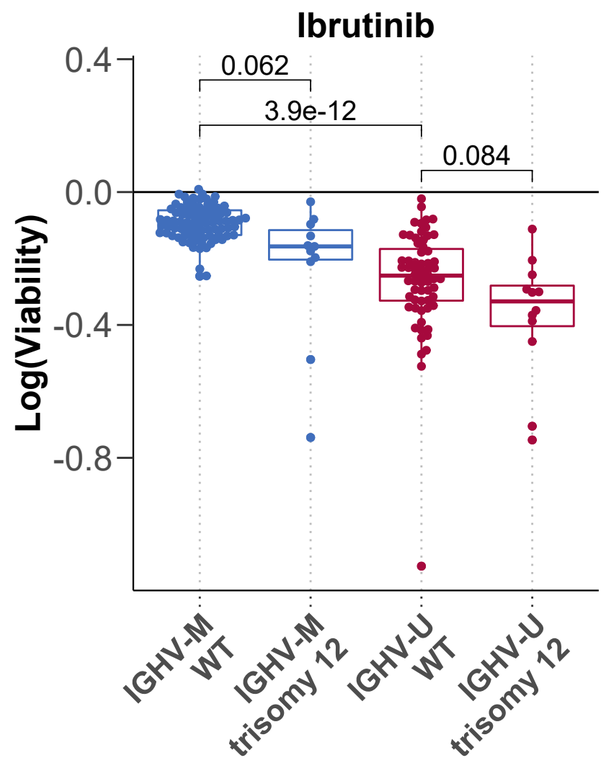

C

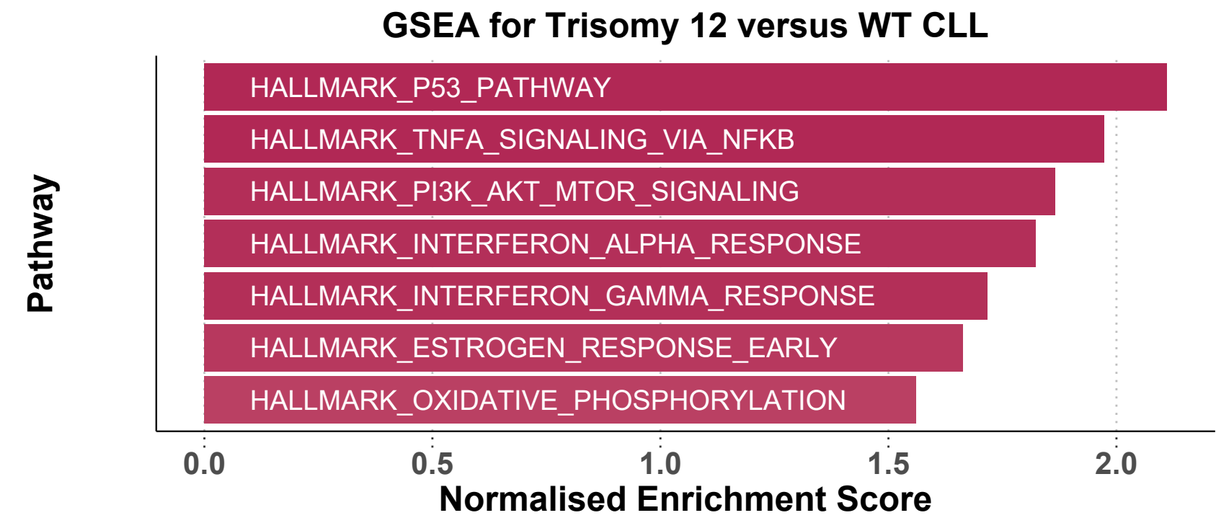

D

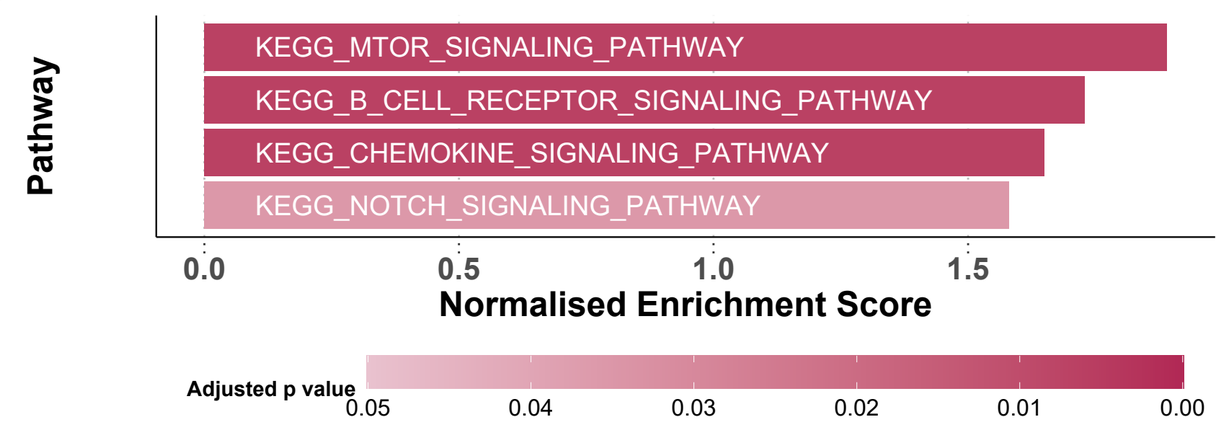

E

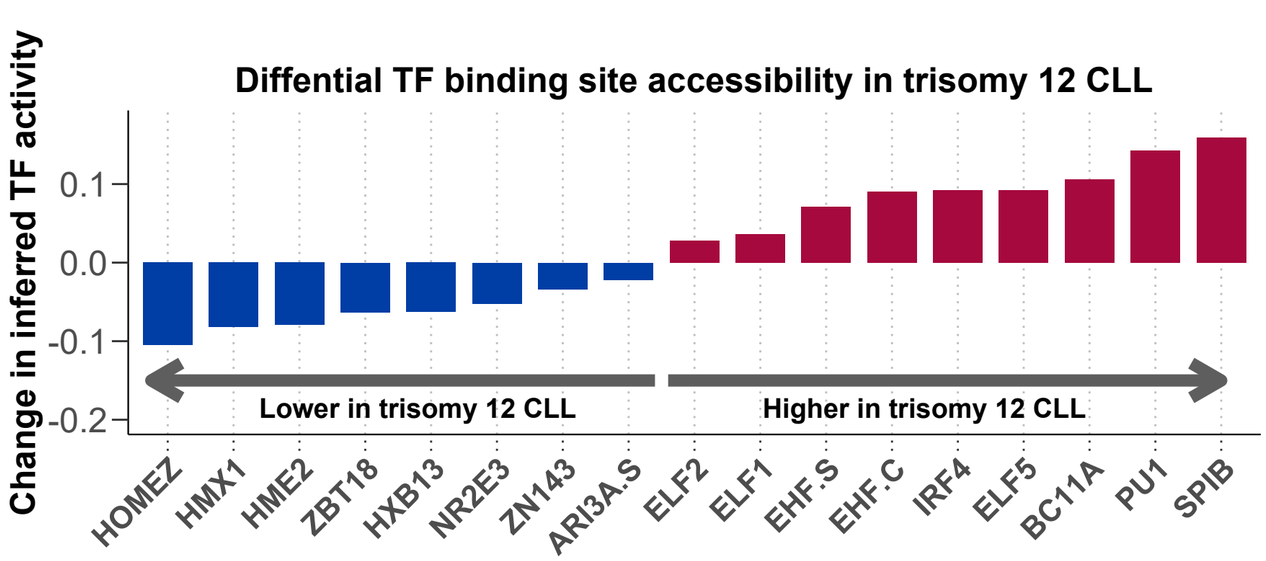

F

Pathway	Geneset Database	Geneset Size	Spi-B targets (/3253)	SPIB p-value
BCR Signaling Pathway	KEGG	75	36	0.000
TLR Signaling Pathway	KEGG	102	40	0.000
Signaling by TGFbeta Receptor Complex	Reactome	73	26	0.007

G

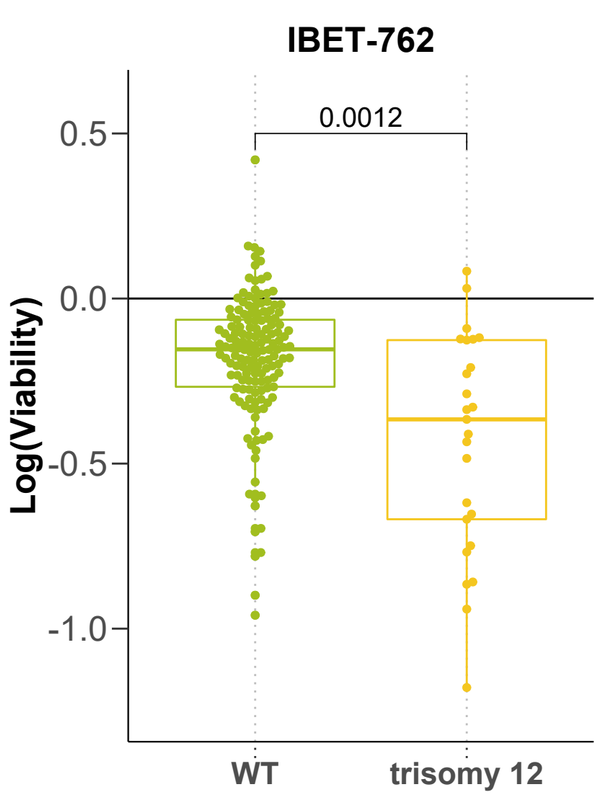

H

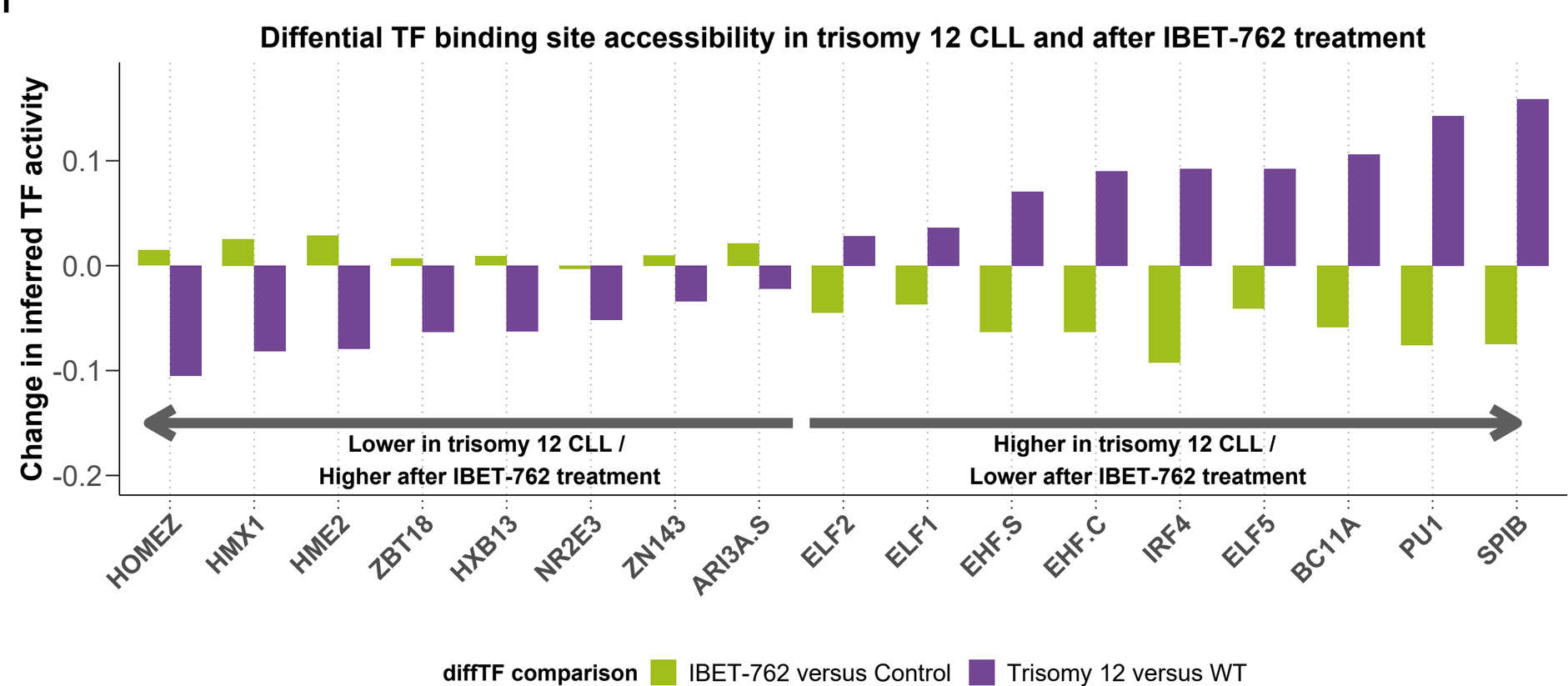

Figure 4. Trisomy 12 modulates responses to microenvironmental signals.

(A+B) Log normalised viability after treatment with resiquimod (TLR 7/8 stimulus) (A) and ibrutinib (B) in the genetic subgroups of IGHV status and trisomy 12. P-values from Student's t-tests.

(C+D) GSEA comparing trisomy 12 samples to non-trisomy 12 samples in Hallmark genesets (C) and selected KEGG genesets of microenvironmental signalling pathways (D).

(E) Differential TF accessibility (y axis) between trisomy 12 (n = 9) and non-trisomy 12 (n = 43) samples, data taken from Rendeiro et al[32]. TFs with adjusted p-value <0.05 are shown and ordered by change in inferred TF activity (x-axis). Spi-B and PU.1 TF binding sites show higher accessibility in trisomy 12 CLL.

(F) Over-representation tests of selected KEGG and Reactome pathways in ChIPseq analysis of Spi-B binding in lymphoma cell lines indicates involvement in coordinating transcriptional response to microenvironmental signals, including BCR and TLR signalling.

(G) Log normalised viability after treatment with the bromodomain inhibitor IBET-762 in trisomy 12 and non-trisomy 12 samples. P-value from Student's t-tests.

(H) Differential TF binding site accessibility (y axis) in trisomy 12 vs non-trisomy 12 CLL samples (purple) and for IBET-762 vs DMSO treated CLL samples (green). Direction of differential accessibility values are shown for two independent datasets comparing trisomy 12 vs non-trisomy 12 CLL and IBET-762 vs control-treated CLL, for all TFs with adjusted p value <0.05 in the trisomy 12 comparison. Absolute change in TF accessibility can not be compared between the two experiments.

Figure 5

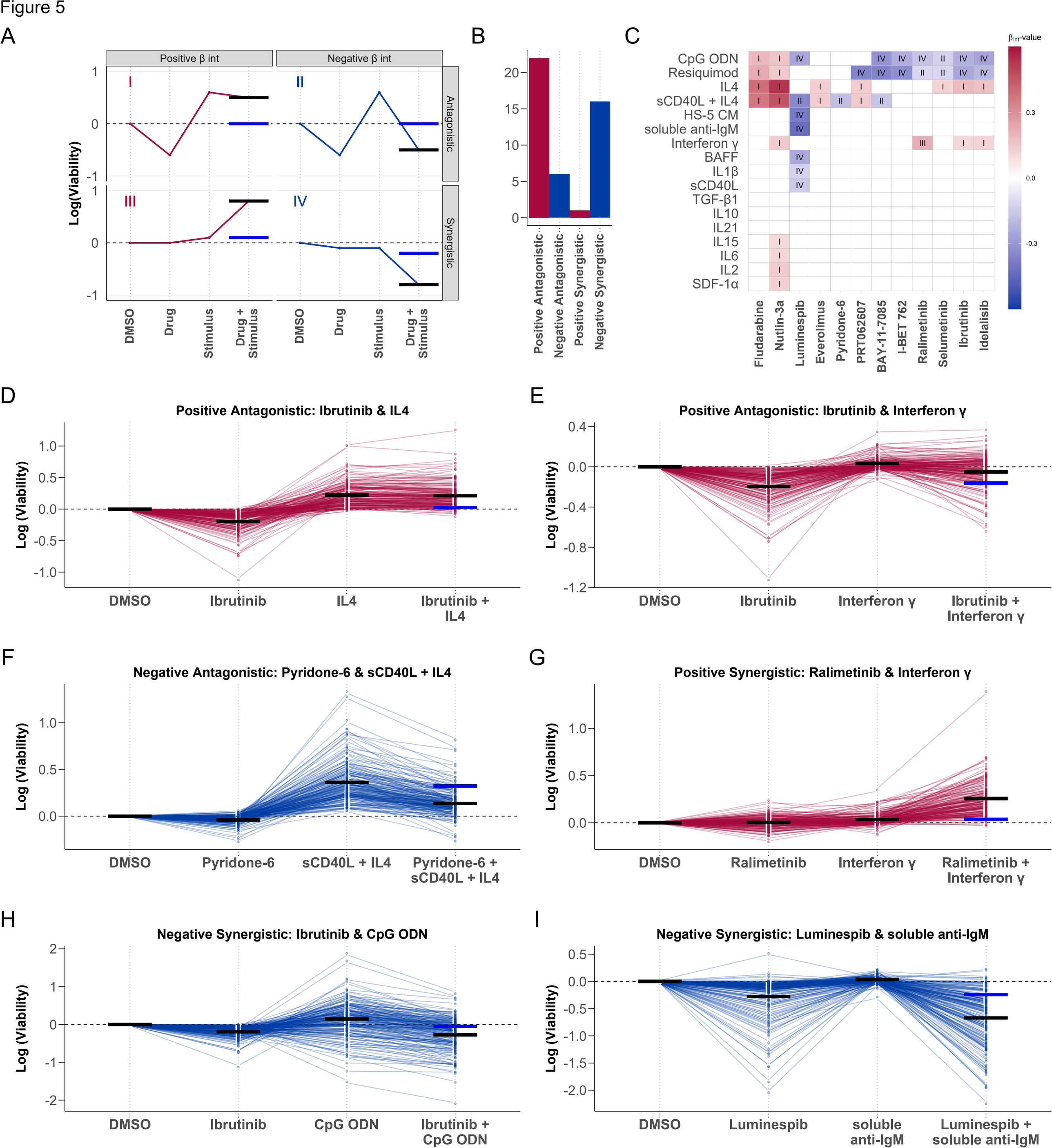
A
Positive β int
Negative β int
Antagonistic
Synergistic
I
II
III
IV
Log(Viability)
DMSO
Drug
Stimulus
Drug + Stimulus
B
Positive Antagonistic
Negative Antagonistic
Positive Synergistic
Negative Synergistic
C
βint-value
CpG ODN
Resiquimod
IL4
sCD40L + IL4
HS-5 CM
soluble anti-IgM
Interferon γ
BAFF
IL1β
sCD40L
TGF-β1
IL10
IL21
IL15
IL6
IL2
SDF-1α
Fludarabine
Nutlin-3a
Luminespib
Everolimus
Pyridone-6
PRT062607
BAY-11-7085
I-BET 762
Ralimetinib
Selumetinib
Ibrutinib
Idelalisib
D
Positive Antagonistic: Ibrutinib & IL4
Log (Viability)
DMSO
Ibrutinib
IL4
Ibrutinib + IL4
E
Positive Antagonistic: Ibrutinib & Interferon γ
Log (Viability)
DMSO
Ibrutinib
Interferon γ
Ibrutinib + Interferon γ
F
Negative Antagonistic: Pyridone-6 & sCD40L + IL4
Log (Viability)
DMSO
Pyridone-6
sCD40L + IL4
Pyridone-6 + sCD40L + IL4
G
Positive Synergistic: Ralimetinib & Interferon γ
Log (Viability)
DMSO
Ralimetinib
Interferon γ
Ralimetinib + Interferon γ
H
Negative Synergistic: Ibrutinib & CpG ODN
Log (Viability)
DMSO
Ibrutinib
CpG ODN
Ibrutinib + CpG ODN
I
Negative Synergistic: Luminespib & soluble anti-IgM
Log (Viability)
DMSO
Luminespib
soluble anti-IgM
Luminespib + soluble anti-IgM

Figure 5. Microenvironmental stimuli influence ex-vivo drug response.

(A) Graphical representation of the four drug-stimulus interaction categories. Categories are defined according to the nature of the interaction (synergistic or antagonistic), and whether the viability is increased or decreased by the stimulus (positive or negative). x-axis shows treatment type, y-axis shows viability with each treatment. Red and blue points and lines depict a representative treatment response pattern for given interaction type. Blue horizontal lines represent the expected viability for combinatorial treatment in the absence of an interaction between drug-stimulus (i.e. additive effects), black horizontal lines represent the measured viability after combinatorial treatment. The difference between the black and blue lines represents the drug - stimulus interaction.

(B) Bar plot of significant interactions in all four categories (p-value for β_{int} is <0.05).

(C) Heatmap of all βint values for which p-value <0.05 for drug-stimulus combinations, annotated with interaction type. Scale indicates size and sign of βint. Rows and columns clustered according to hierarchical clustering.

I: Positive β_{int} and antagonistic (Microenvironmental stimulation reduces drug effect)

II: Negative β_{int} and antagonistic (Drug reduces stimuli effect)

III: Positive β_{int} and synergistic (Microenvironmental stimulation and drug have synergistic pro-survival effect)

IV: Negative β_{int} and antagonistic (Microenvironmental stimulation and drug show synergistic toxicity)

(D - I) Examples of drug-stimulus interactions, for each category. Plots show log transformed viability values with each treatment, for all samples. Each line represents one patient sample linked across treatments. Black lines in single treatments indicate viability predicted by the linear model. In combinatorial treatment, the expected viability based on the additive effect of drug and stimulus (blue), and the viability with interaction (black), are shown to indicate the impact of the interaction.

(D+E) Ibrutinib, a clinically used BTK inhibitor, is blocked by IL4 and IFNγ.

(F) The JAK inhibitor pyridone-6 inhibits the pro-survival effect of sCD40L + IL4 stimulation.

(G) The p38 inhibitor ralimetinib and IFNγ show a synergistic pro-survival effect not seen in either single treatment.

(H) TLR agonists, including CpG ODN (shown) increase sensitivity to BTK inhibition by ibrutinib, despite increasing viability as single treatments.

(I) Soluble anti-IgM sensitises CLL samples to HSP90 inhibition by luminespib.

Figure 6

A

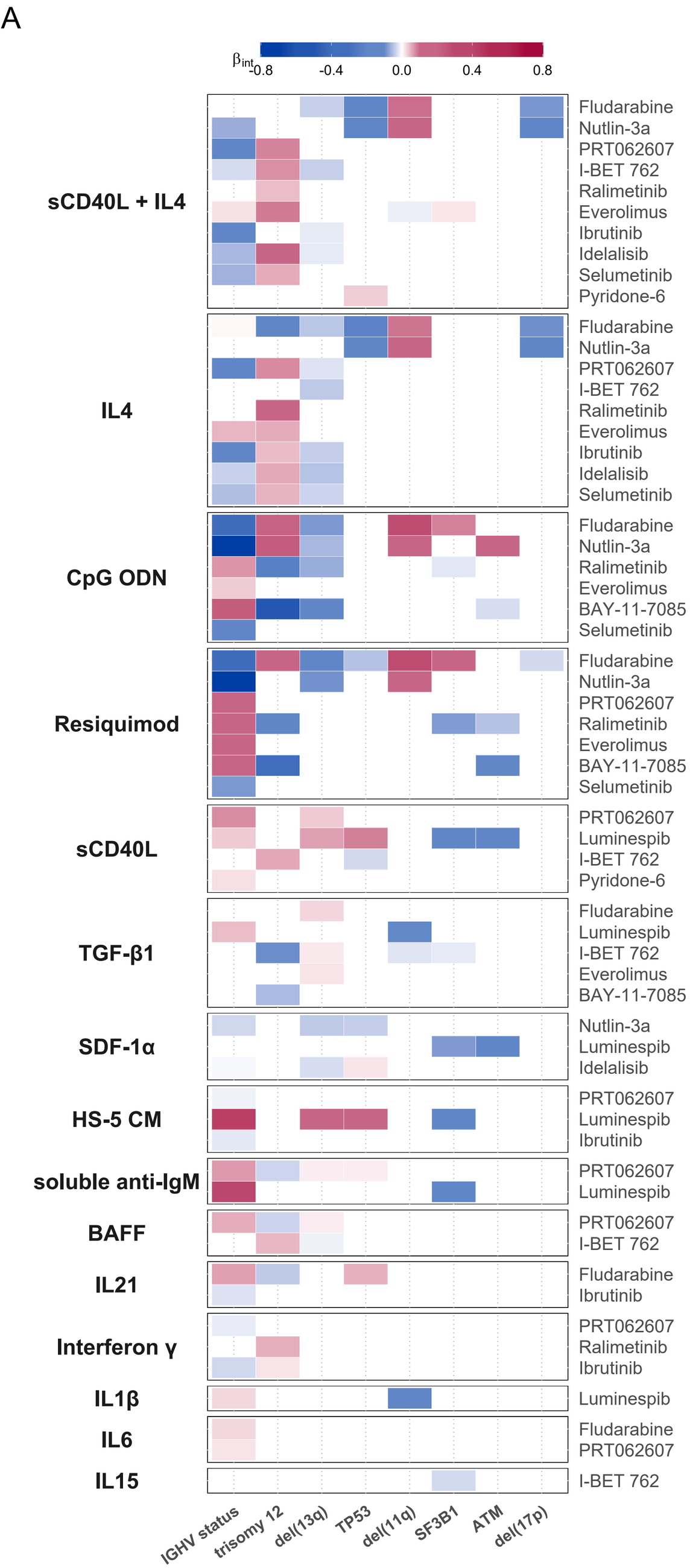

B

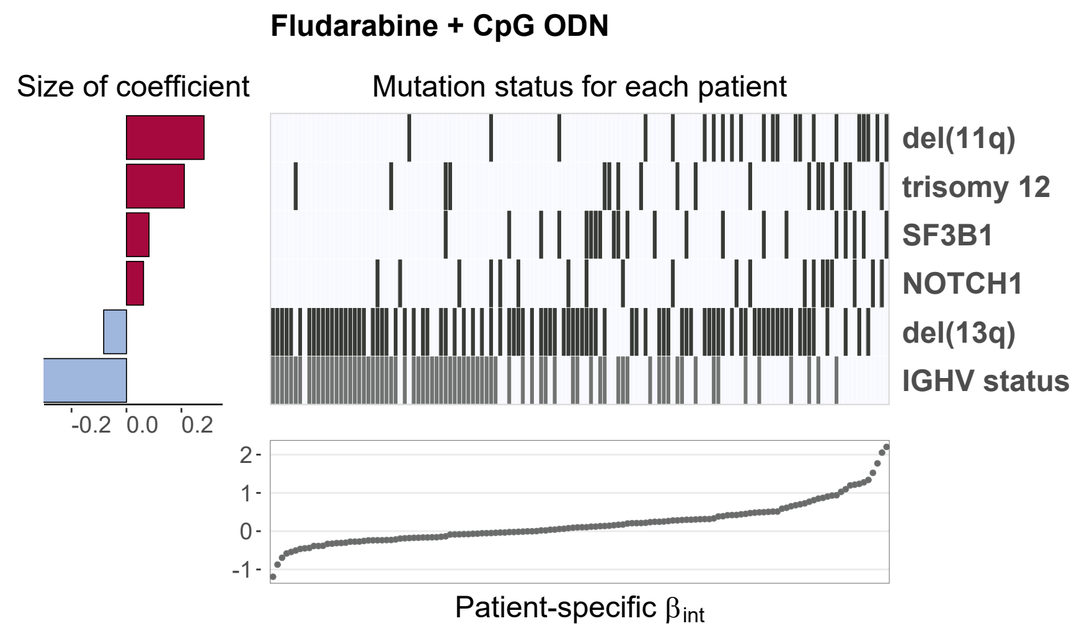

C

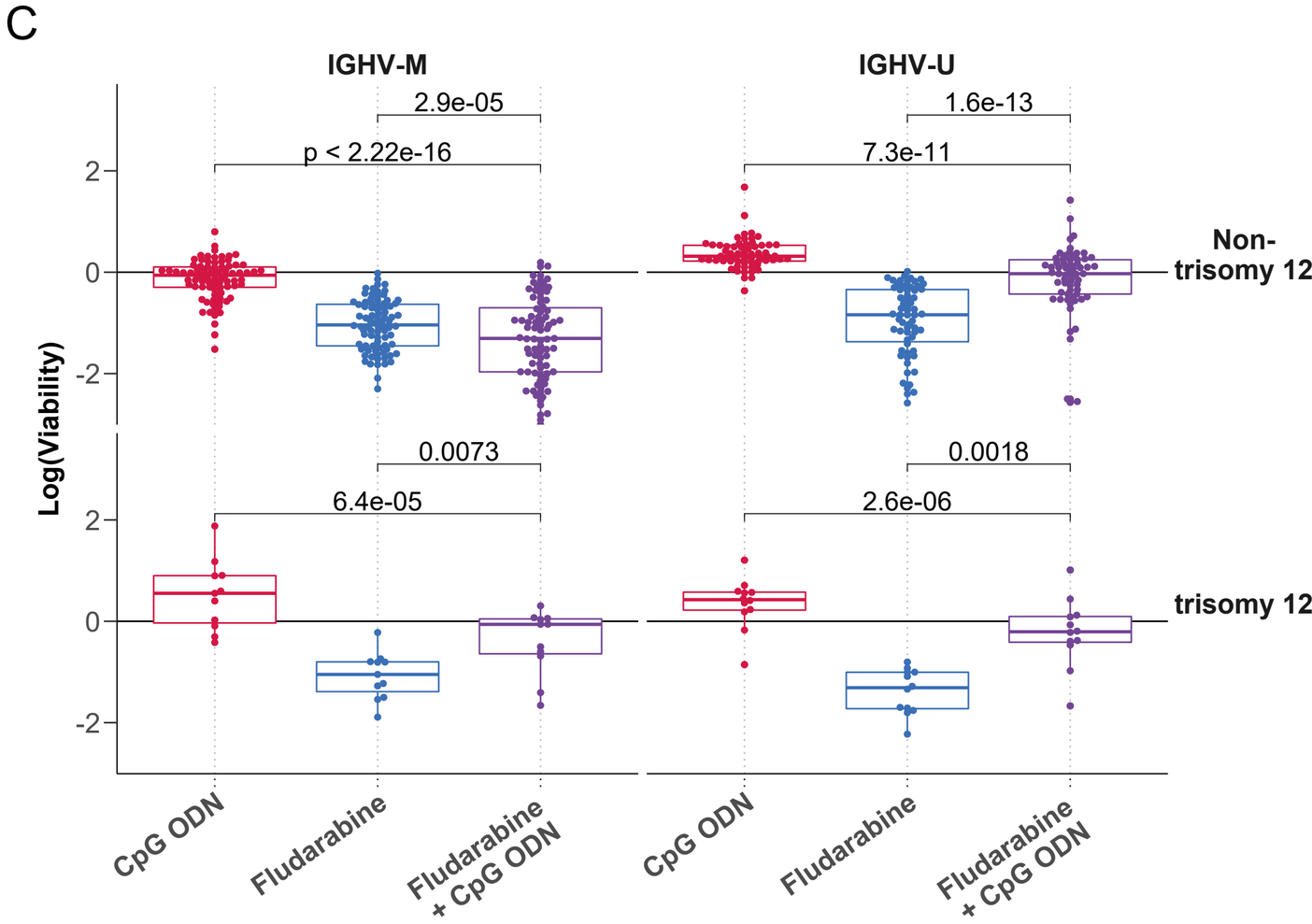

D

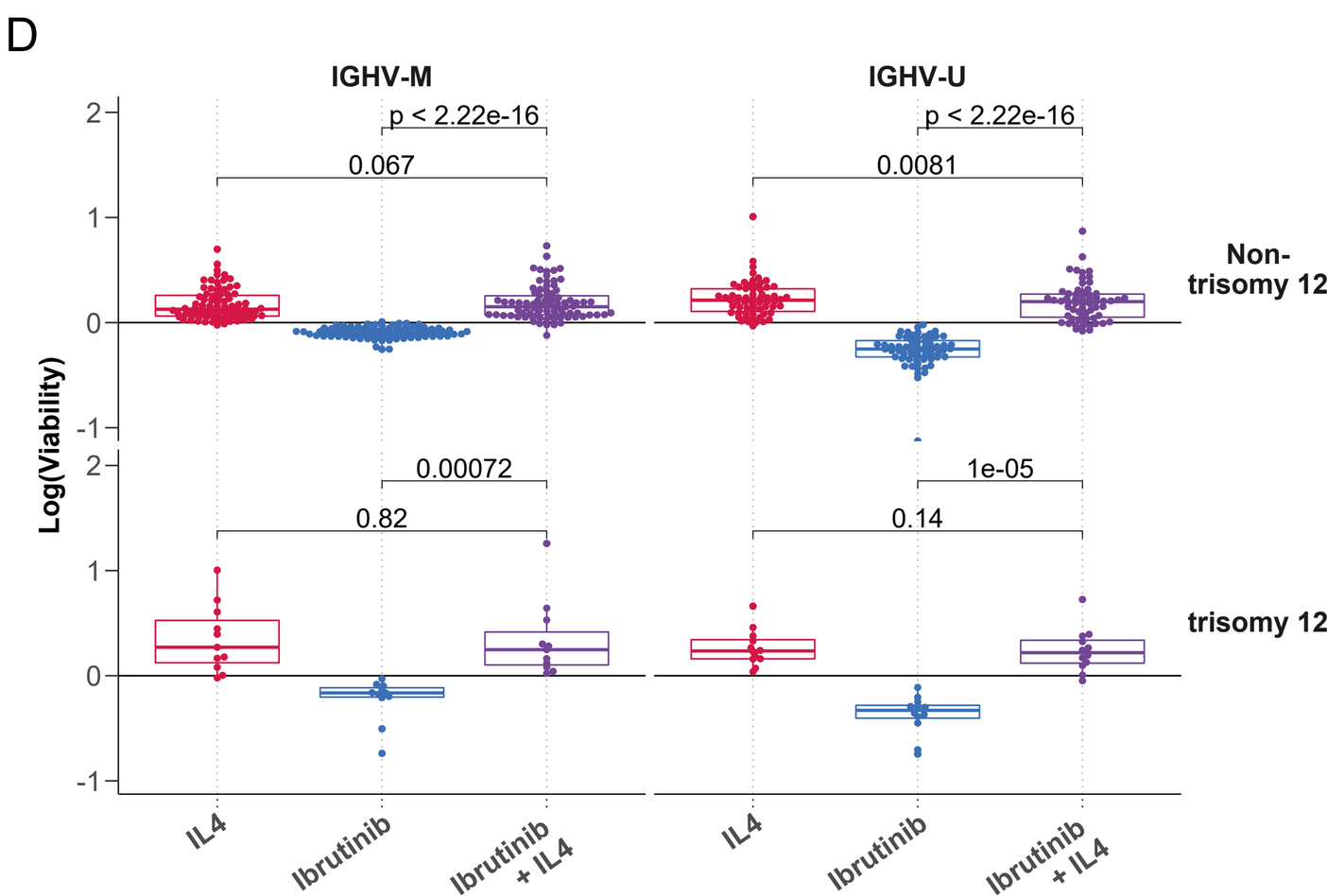

Figure 6. Integrating the effects of genetic features and stimuli on drug response.

(A) Heatmap depicting the eight most commonly selected genetic predictors of drug-stimulus interactions (each row represents the coefficients of a single multivariate model, as in (B)). Stimuli are shown on left, and corresponding drugs on right. Coloured fields indicate that βint for given drug and stimulus is modulated by corresponding genetic feature. Positive coefficients are shown in red, indicating a more positive β_{int} if the feature is present. Drug-stimulus combinations with no genetic predictors of β_{int} amongst shown genetic factors are omitted for clarity.

(B) Predictor profile depicting genetic features that modulate the interaction between fludarabine and CpG ODN. The horizontal bars on left show the size of fitted coefficients assigned to genetic features. The matrix in the centre indicates patient mutation status for the selected genetic features aligned with the scatter plot indicating the size of βint for each patient. Grey lines indicate the presence of genetic feature/IGHV mutated.

(C-D) Beeswarm boxplots of log(viability) values, for fludarabine + CpG ODN (C) and ibrutinib + IL4 (D) single and combinatorial treatments, faceted by IGHV status and trisomy 12 status. P-values from paired Student's t-tests.

Figure 7

A

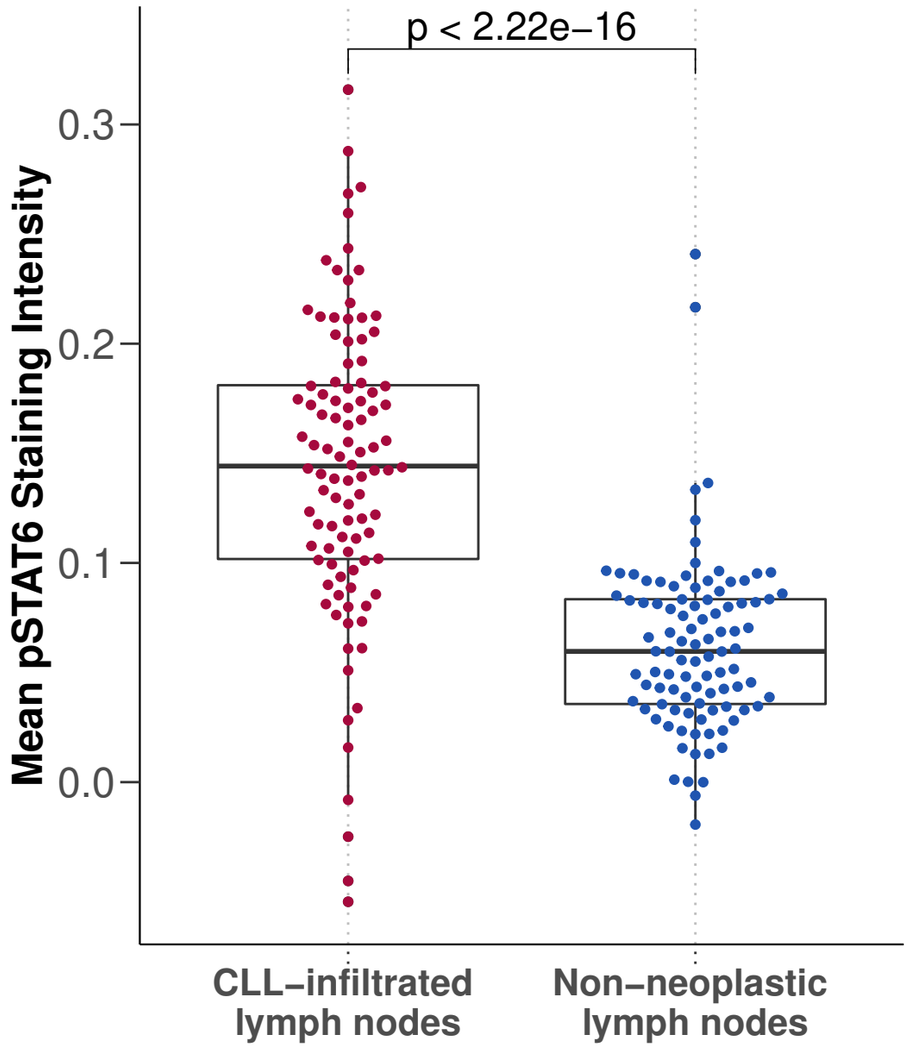

C

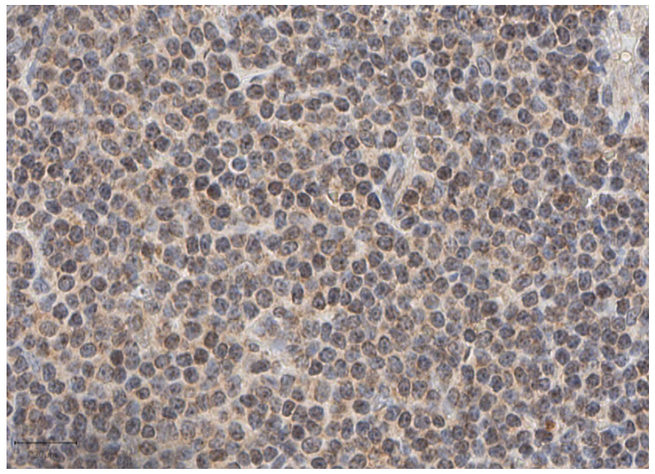

D

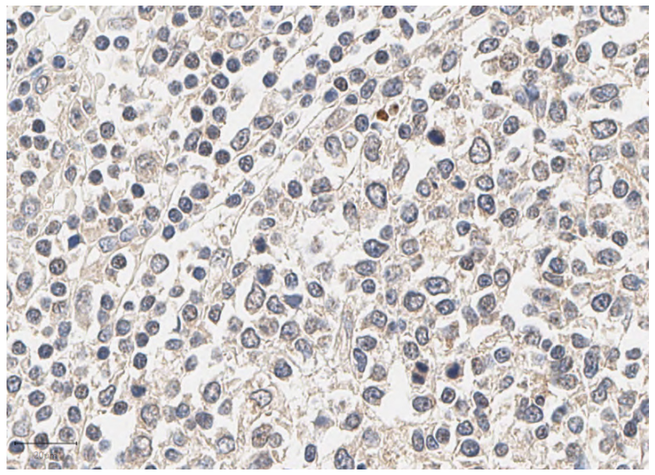

G

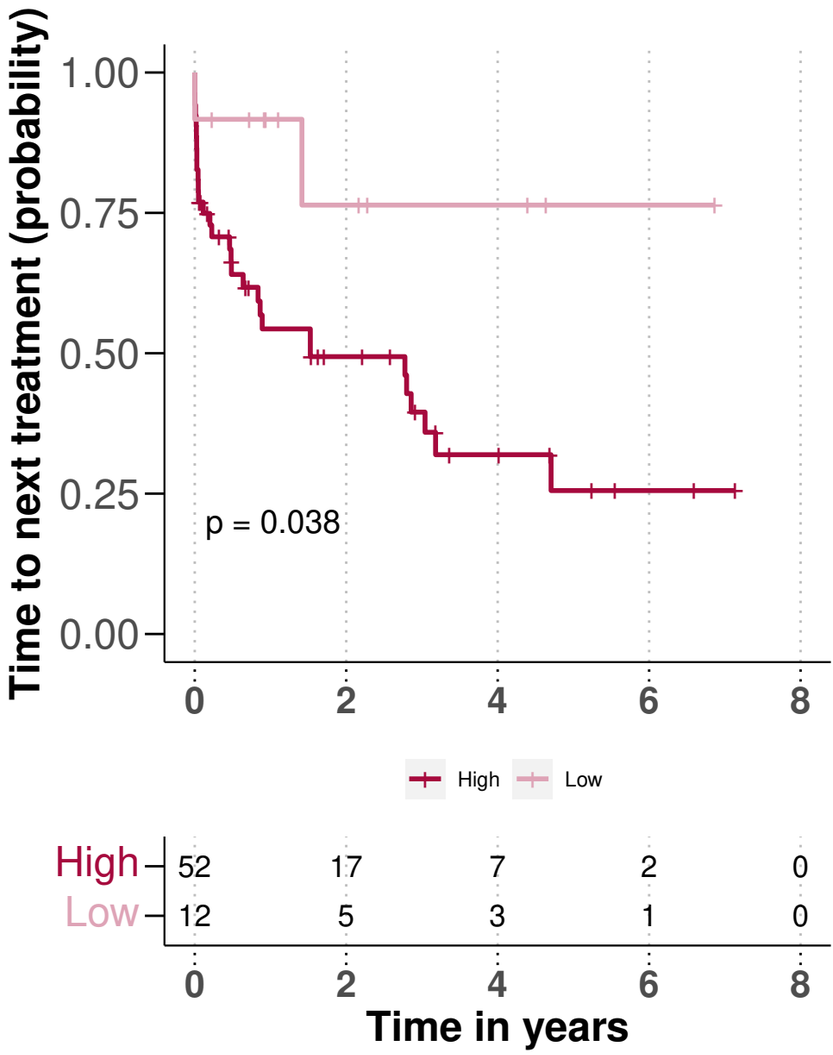

B

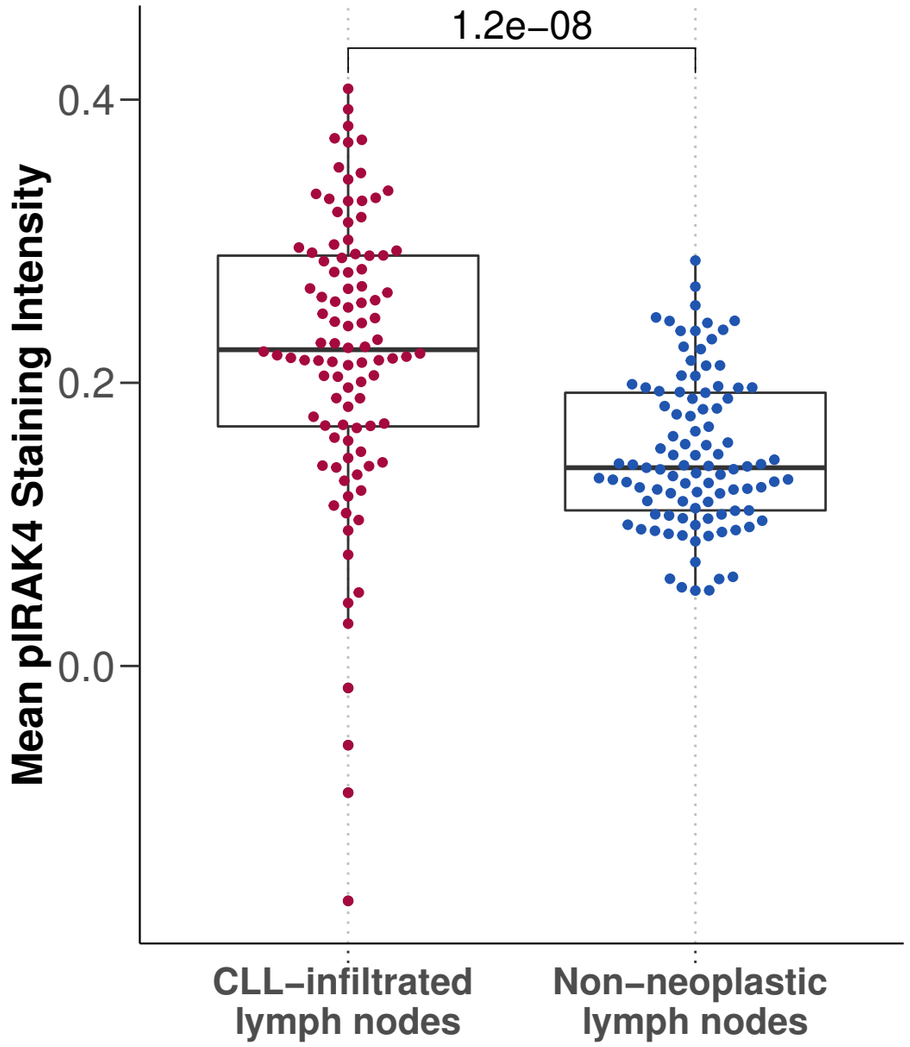

E

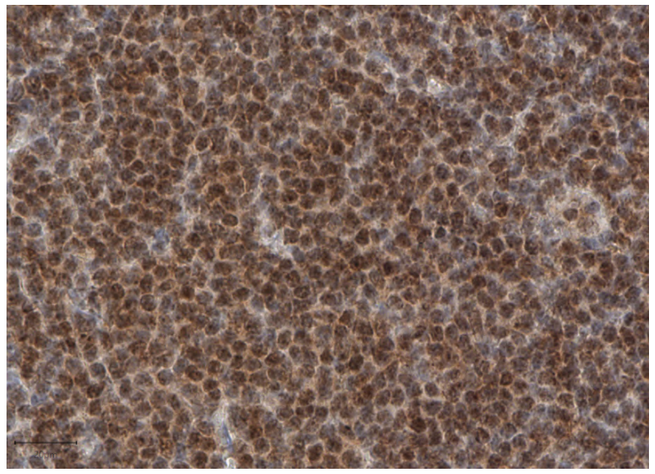

F

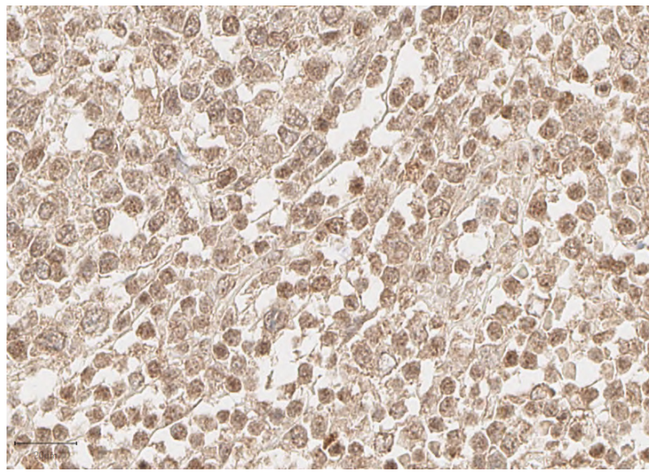

H

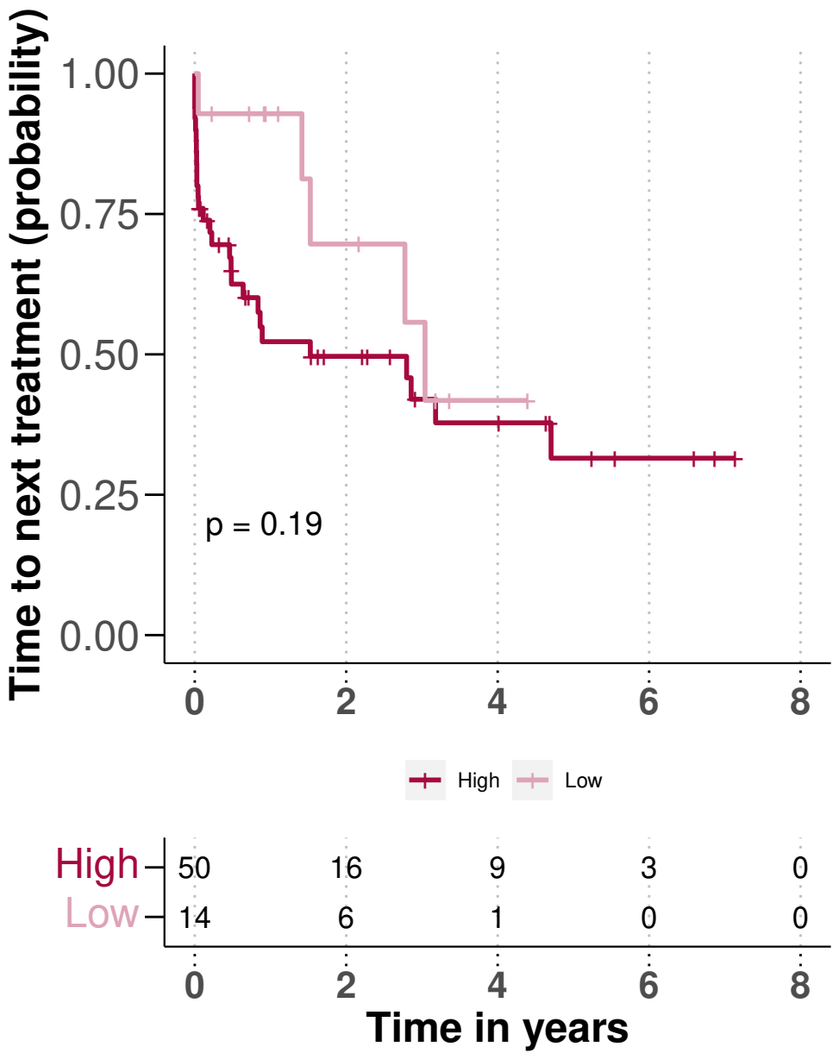

Figure 7. IL4 and TLR signalling are upregulated in CLL-infiltrated lymph nodes.

(A-B) Mean pSTAT6 (A) and pIRAK4 (B) staining intensity in CLL-infiltrated and non-neoplastic lymph node biopsies after background subtraction (y axis), p-values from Student's t-test. Each dot represents the mean of all cells in TMA cores per patient sample.

(C-F) Example images of IHC sections.

(C + D) show pSTAT6 levels in (C) CLL-infiltrated and (D) non-neoplastic samples.

(E + F) show pIRAK4 levels in (E) CLL-infiltrated and (F) non-neoplastic samples.

(G + H) Kaplan-Meier plots for time to next treatment stratified by levels (high / low) of pSTAT6 (G) and pIRAK4 (H).